Neuroscience 122 (2003) 811–829

SYNAPTIC BACKGROUND NOISE CONTROLS THE INPUT/OUTPUT CHARACTERISTICS OF SINGLE CELLS IN AN *IN VITRO* MODEL OF *IN VIVO* ACTIVITY

J.-M. FELLOUS,[a]* M. RUDOLPH,[b] A. DESTEXHE[b] AND T. J. SEJNOWSKI[a,c]

[a]*Computational Neurobiology Laboratory, Howard Hughes Medical Institute, The Salk Institute for Biological Studies, 10010 North Torrey Pines Road, La Jolla, CA 92037, USA*

[b]*Unité de Neurosciences Intégratives et Computationelles, CNRS, 1 Avenue de la Terrasse, 91198 Gif-sur-Yvette, France*

[c]*Division of Biological Sciences, University of California, San Diego, La Jolla, CA 92093, USA*

Abstract—*In vivo*, *in vitro* and computational studies were used to investigate the impact of the synaptic background activity observed in neocortical neurons *in vivo*. We simulated background activity *in vitro* using two stochastic Ornstein-Uhlenbeck processes describing glutamatergic and GABAergic synaptic conductances, which were injected into a cell in real time using the dynamic clamp technique. With parameters chosen to mimic *in vivo* conditions, layer 5 rat prefrontal cortex cells recorded *in vitro* were depolarized by about 15 mV, their membrane fluctuated with a S.D. of about 4 mV, their input resistances decreased five-fold, their spontaneous firing had a high coefficient of variation and an average firing rate of about 5–10 Hz. Brief changes in the variance of the α-amino-3-hydroxy-5-methyl-4-isoxazolepropionic acid (AMPA) synaptic conductance fluctuations induced time-locked spiking without significantly changing the average membrane potential of the cell. These transients mimicked increases in the correlation of excitatory inputs. Background activity was highly effective in modulating the firing-rate/current curve of the cell: the variance of the simulated γ-aminobutyric acid (GABA) and AMPA conductances individually set the input/output gain, the mean excitatory and inhibitory conductances set the working point, and the mean inhibitory conductance controlled the input resistance. An average ratio of inhibitory to excitatory mean conductances close to 4 was optimal in generating membrane potential fluctuations with high coefficients of variation. We conclude that background synaptic activity can dynamically modulate the input/output properties of individual neocortical neurons *in vivo*.

Key words: dynamic-clamp, computational model, gain, variance detection, synapse.

The response of cortical neurons *in vivo* to a repeated sensory stimulus is highly variable (Softky and Koch, 1993; Holt et al., 1996; Shadlen and Newsome, 1998). Since the spike generating mechanism *in vitro* shows considerably more reliability and precision than observed *in vivo* (Mainen and Sejnowski, 1995; Fellous et al., 2001), most of the *in vivo* variability is likely due to the variability of synaptic inputs (Zador, 1998). The level of synaptic background noise has significant consequences for the input/output characteristics of an individual cortical neuron and affects its ability to detect transient or sustained input signals (Destexhe and Paré, 1999; Destexhe et al., 2003).

Correlated firing in small groups of neurons may occur in response to a stimulus (Sejnowski, 1976; Gawne and Richmond, 1993; Shadlen and Newsome, 1998; Bair, 1999; Bazhenov et al., 2001) and may be modulated by attention (Steinmetz et al., 2000; Fries et al., 2001; Salinas and Sejnowski, 2001). Recent computational studies indicate that the synaptic correlations resulting from a sustained increase in presynaptic synchrony may significantly modulate the incoming synaptic noise statistics and can influence the firing rate and the firing variability of a postsynaptic neuron (Salinas and Sejnowski, 2000; Svirskis and Rinzel, 2000; Tiesinga et al., 2000). In many cortical systems however, signals are transient rather than sustained. In the visual cortex for example, visual stimuli produce transient synchronization lasting tens of milliseconds in subpopulations of neurons (Zador, 1999; Fabre-Thorpe et al., 2001; Keysers et al., 2001; Reinagel and Reid, 2002). Cortical neurons should be capable of detecting these increases in input correlation despite intrinsic membrane noise and background synaptic activity as predicted by modeling studies (Rudolph and Destexhe, 2001). It has been difficult to experimentally assess the correlation detection ability of a cell mainly because the classical techniques do not allow for the manipulation of the level of correlation between synaptic inputs. Recently Chance et al. (2002) have explored these issues *in vitro* using a dynamic clamp. We extend these results by independently varying the magnitudes and variability of the excitatory and inhibitory conductances injected into neurons.

A precise characterization of synaptic background activity based on intracellular recordings *in vivo* was only possible in preparations where the animal is anesthetized (Paré et al., 1998). In this condition, the magnitude and time structure of synaptic inputs cannot be easily manipulated, and the neurochemical environment of a neuron cannot be easily monitored. In an *in vitro* preparation however, precise control of the stimulation patterns, a tight control of the neurochemical environment, and a realistic level of intrinsic membrane noise are possible. However,

*Corresponding author. Tel: +1-858-453-4100x1618; fax: +1-858-587-0417.
E-mail address: fellous@salk.edu (J.-M. Fellous).

Abbreviations: GABA, γ-aminobutyric acid; AMPA, α-amino-3-hydroxy-5-methyl-4-isoxazolepropionic acid; CV, coefficient of variation; ISI, inter-spike interval; IT, inferotemporal cortex; OU, Ornstein-Uhlenbeck; SNR, signal-to-noise ratio.

0306-4522/03$30.00+0.00
doi:10.1016/j.neuroscience.2003.08.027

neurons *in vitro* have a greatly diminished amount of spontaneous synaptic activity because of the slicing procedure and their membrane potentials typically remain constant well below threshold. In contrast, spontaneous synaptic inputs *in vivo* can produce on average a membrane depolarization of about 15 mV, voltage fluctuations of 10 mV in amplitude (4 mV S.D.), an 80% decrease in input resistance, and a baseline discharge (2–10 Hz) with a high coefficient of variation (Paré et al., 1998; Destexhe and Paré, 1999; Destexhe et al., 2003).

In order to study the input/output characteristics of neurons that receive background synaptic noise, we used the dynamic clamp technique (Sharp et al., 1993) to create a real-time interface between a neuron recorded *in vitro* and a computer model of *in vivo* synaptic background activity. In this hybrid preparation, the stimulation of a neuron and its neurochemical environment can be tightly controlled, the intrinsic membrane noise is intact, and simulated background *in vivo*-like synaptic noise is injected into the neuron. Synaptic background activity can be explicitly simulated by large numbers of excitatory and inhibitory synapses that release randomly (Bernander et al., 1991; Destexhe and Paré, 1999; Svirskis and Rinzel, 2000; Tiesinga et al., 2000). Previous work has shown that, at the soma, the synaptic input resulting from the activation of thousands of inhibitory and excitatory synaptic conductances distributed throughout the dendritic tree is statistically equivalent to two independent fluctuating point-conductance injections modeled as Ornstein-Uhlenbeck (OU) stochastic processes (Destexhe et al., 2001, 2003).

In this study, we first investigated the parameter ranges within which synaptic background activity modeled as OU conductances restores *in vivo*-like passive and active properties in cells recorded at their soma *in vitro*. Using a detailed compartment model, we then examined how changes in the correlations of synaptic inputs resulted in predictable changes in the variance of the membrane potential voltage at the soma. This change in variance can be simulated in a point-conductance model by changing the variance of the stochastic process describing excitatory inputs. In order to investigate transient changes in synchrony in cells receiving continuous synaptic background inputs, we studied the spiking probability of cells in response to brief changes in the variance of this stochastic process. Finally, we examined the firing rate sensitivity to sustained current injections (firing-rate vs. current (F-I) curve) as a function of the mean and variance of the simulated synaptic background activity.

EXPERIMENTAL PROCEDURES

In vivo experiments

The methods used in the *in vivo* preparations are similar to those described elsewhere (Henze et al., 2000). Three Sprague–Dawley rats (300–500 g) were anesthetized with urethane (1.65 g/kg; Sigma) and placed in a stereotaxic apparatus (Kopf, Tujunga, CA, USA). The body temperature of the rat was monitored and kept around 35 °C. A small portion of the skull was drilled (about 1 mm×1 mm) above the pre-limbic/infra-limbic areas of the prefrontal cortex (2.0 mm anterior from Bregma, 1.0 mm lateral, in either hemisphere) and cells were recorded about 3 mm below the surface. The dura mater was carefully punctured to expose the brain tissue. A 0.9% NaCl solution was used to keep the opening moist. Intracellular recordings were obtained using 1.8 mm or 2.0 mm capillary glass (Sutter Instrument Inc., Novato, CA, USA) filled with 1 M potassium acetate (80–120 MΩ, determined using bridge balancing). Once the electrode tip was placed in contact with the brain, the hole was filled with a mixture of paraffin (50%) and paraffin oil (50%) to prevent the drying of the brain and to decrease pulsations. The electrode was then advanced using a Sutter MP-285 micromanipulator (depth: 1.0 mm–4.0 mm) to obtain intracellular recordings. Amplification was achieved using an Axoclamp 2A amplifier (Axon Instruments, Foster City, CA, USA) in current clamp mode and data were digitized using a PCI16-E1 data acquisition board (National Instrument, Austin, TX, USA). Data acquisition rate was 10 kHz. Six putative pyramidal cells were recorded (regularly spiking with adapting responses to current pulses). Two of these cells exhibited up and down states. Because these states are driven by structured synaptic activity (Lewis and O'Donnell, 2000) they were not considered in a state of 'background' synaptic activity, and were discarded from our analysis. The four other cells were used in this study.

In vitro experiments

Coronal slices of rat pre-limbic and infra limbic areas of prefrontal cortex were obtained from 2–4 week old Sprague–Dawley rats. Rats were anesthetized with Isoflurane (Abbott Laboratories, IL, USA) and decapitated. Their brain were removed and cut into 350 μm thick slices using standard techniques. Patch-clamp was performed under visual control at 30–32 °C. In most experiments Lucifer Yellow (RBI; 0.4%) or Biocytin (Sigma; 0.5%) was added to the internal solution. In some experiments, synaptic transmission was blocked by D-2-amino-5-phosphonovaleric acid (50 μM), 6,7-dinitroquinoxaline-2,3, dione (10 μM), and bicuculline methiodide (20 μM). All drugs were obtained from RBI or Sigma, freshly prepared in ACSF and bath applied. Whole cell patch-clamp recordings were achieved using glass electrodes (4–10 MΩ) containing (mM: $KmeSO_4$, 140; HEPES, 10; NaCl, 4; EGTA, 0.1; Mg-ATP, 4; Mg-GTP, 0.3; phosphocreatine 14). Data were acquired in current clamp mode using an Axoclamp 2A amplifier. Extracellular stimulation (Fig. 1B) was conducted with a large tip (100 μm) bipolar electrode (FHC, Bowdoinham, ME, USA) placed between layers 2/3 and layer 5, about 100 μm away from the cell's main axis. The electrode was attached to an analog stimulus isolation unit (Getting Instruments, IA, USA) commanded by the data acquisition computer (see below). We used regularly spiking layer five pyramidal cells.

All *in vitro* voltage measurement were corrected for the liquid junction potential. This junction potential is negligible when sharp electrodes are used (as in the *in vivo* experiments described above) because the concentration of ions in the electrode is high and because the ions' mobility is similar. For the patch clamp technique however, this junction potential cannot be neglected. In control experiments we measured the junction potential. We first placed the internal solution in the bath and we zeroed the amplifier. We then replaced the bath solution by the standard ACSF and measured the junction potential in current clamp mode. The junction potential was consistently between 8 and 10 mV (9 mV±1; three electrodes, five measurements), so we subtracted 10 mV from all the measurements obtained *in vitro*, in current clamp mode. Details of the estimation and measurements of liquid junction potentials can be found elsewhere (Barry and Lynch, 1991; Barry, 1994; Neher, 1995).

Histology

Cell staining (Fig. 5A, inset) was conducted using a standard diaminobenzidine procedure. Slices were fixed for at least 4 h in a

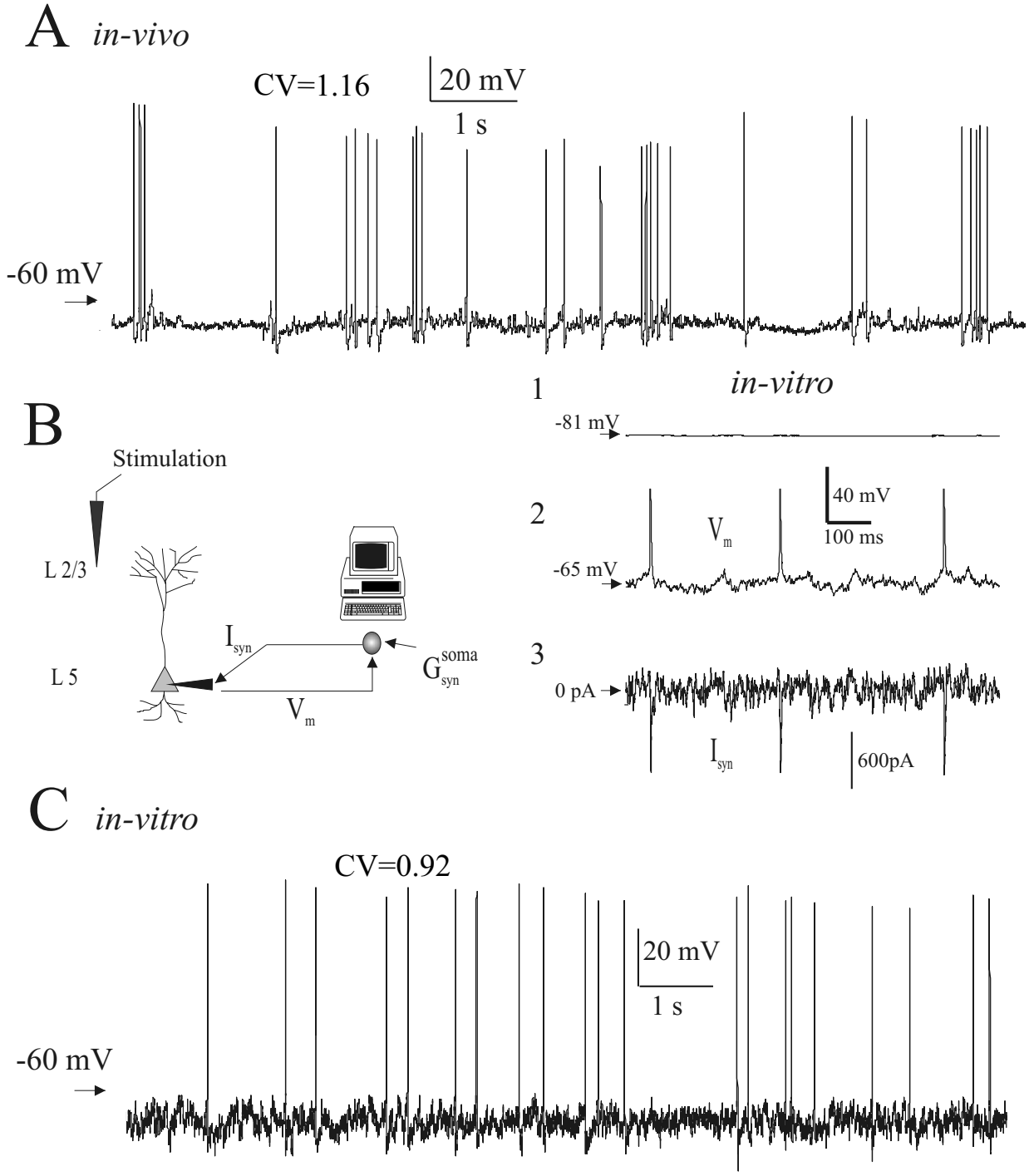

Fig. 1. Simulating synaptic inputs with dynamic clamp. A: *In vivo* recording of a layer 5 pyramidal cell in rat prefrontal cortex. Note the variable pattern of discharges (CV=1.1, average firing rate 2.1 Hz), the large membrane potential fluctuations (S.D. of 4.8 mV) and the level of depolarization (average membrane potential was −66 mV). The input resistance was 38 MΩ. B: Experimental protocol *in vitro*. Dynamic clamp was implemented as a fast loop (0.1–0.83 ms) in current clamp mode: Somatic membrane voltage was read, the instantaneous synaptic conductance was computed and used with the current membrane voltage to produce the synaptic current that was then injected back into the cell. We recorded from layer 5 pyramidal cells, and stimulated in layers 2/3. The right panels show an example of the application of this protocol. Trace 1 shows the membrane voltage of a layer 5 pyramidal cell recorded *in vitro* with no point conductance clamp. The two lower traces show the membrane voltage (V_m, trace 2) resulting from the injection of the synaptic current (I_{syn}, trace 3) computed in real time with the point-conductance model. (Ge_0=5 nS, Gi_0=25 nS, σ_e=5 nS, σ_i=12.5 nS). C: Sample free running voltage trace of a cell *in vitro* undergoing simulated synaptic background activity. The parameters of the point conductance clamp were adjusted to mimic the *in vivo* behavior of the cell in A (Ge_0=5 nS, Gi_0=25 nS, σ_e=3 nS, σ_i=6.2 nS). Input resistance was 41 MΩ, average membrane potential was −65.8 mV, S.D. of the membrane potential fluctuations was 4.6 mV, the CV was 0.92 and average firing rate was 2.5 Hz.

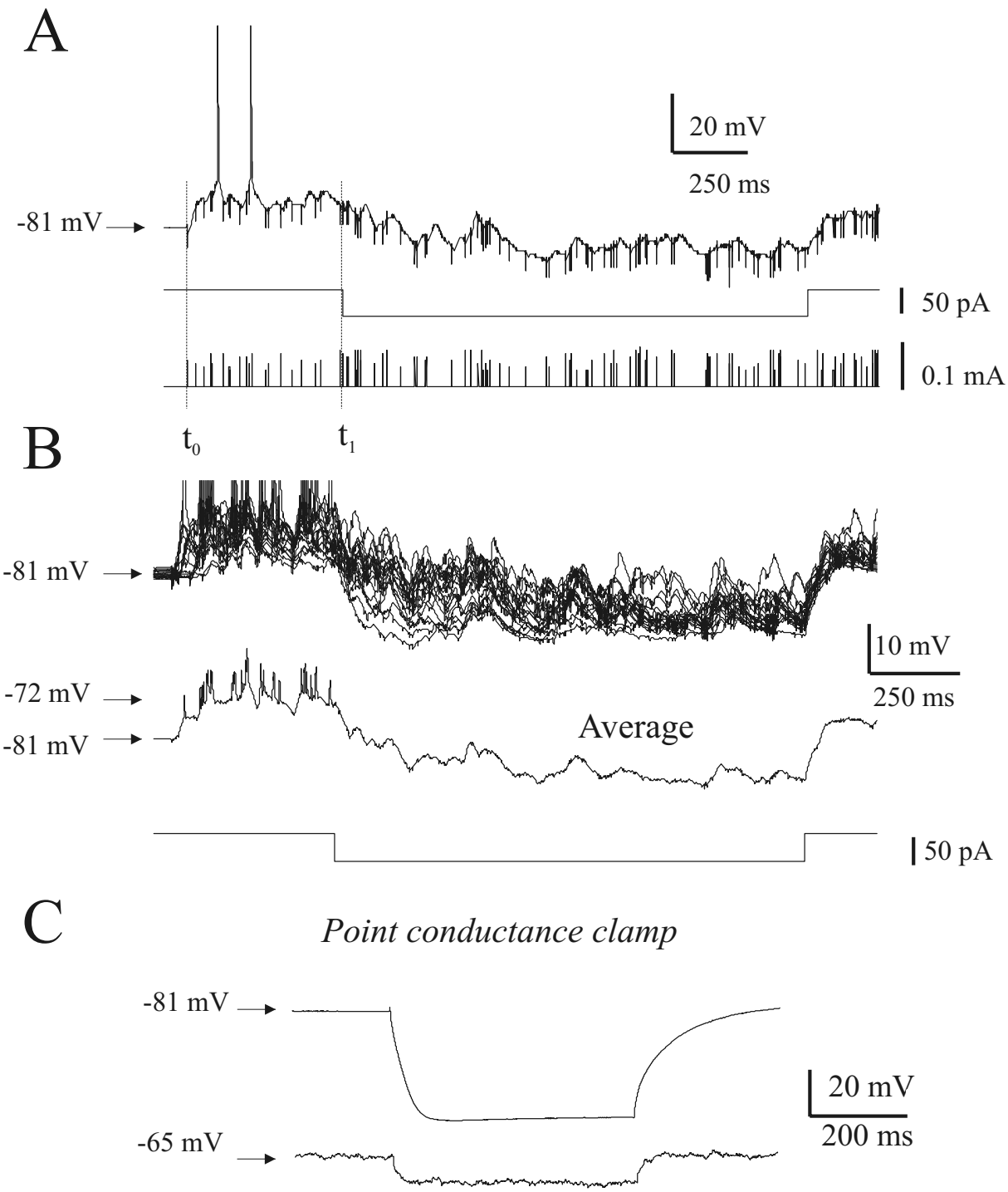

Fig. 2. Reduction in input resistance during actual and simulated synaptic inputs *in vitro*. A: A layer 5 pyramidal cell (V_{rest}, −71 mV) received a train of afferent synaptic stimulation elicited by extracellular stimulations in layers 2/3. The shocks started a t_0, were Poisson distributed at a frequency of 120 Hz, their amplitude was random (gaussian around a mean that elicited a reliable epsp) and their width was 0.3 ms. The cell depolarized to about −62 mV and emitted occasional spikes. At t_1, 500 ms after the train onset, the cell was somatically injected with a current pulse (−50 pA) to evaluate its input resistance. B: Superposed individual traces (top) and average trace (middle) obtained with three different synaptic train patterns (two trains at 120 Hz and one train at 200 Hz, six trials each) in the same cell as in A. Stimulation artifacts have been removed with low-pass filtering (500 Hz) and action potentials are truncated. The I-V curve was constructed by repeated injection of five different hyperpolarizing current pulses amplitudes. Input resistance was obtained as the slope of the linear fit to the I-V curve. During these random synaptic inputs, the resistance of this cell was 185 MΩ, while it was 230 MΩ in the absence of synaptic stimulation (panel C, top). C: Point conductance clamp. The same cell as in A and B was injected with a 200 pA hyperpolarizing pulse. The two traces show the average response (six trials) of the cell in control condition (top) and when it was subjected to the point-conductance clamp (bottom: Ge_0=3 nS, Gi_0=15.5 nS, σ_e=5 nS, σ_i=12.5 nS). The input resistance was reduced from 230 MΩ to 52 MΩ.

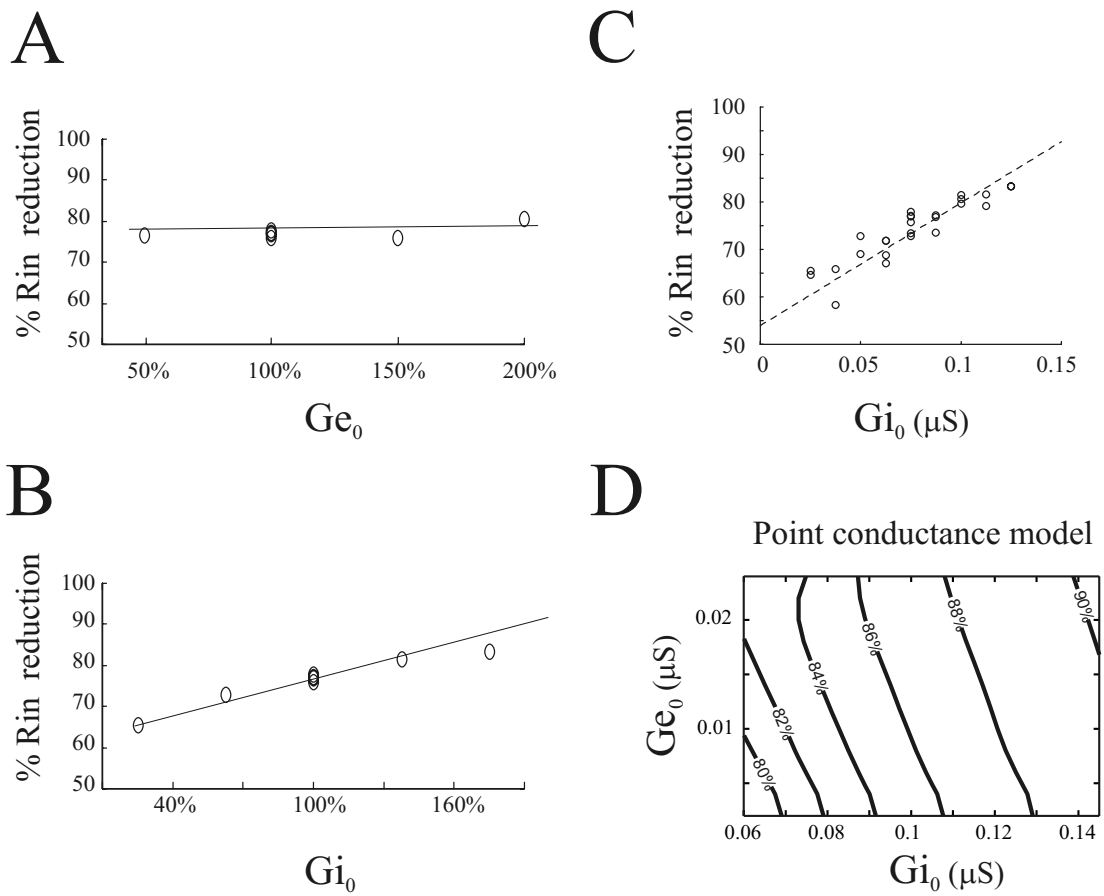

Fig. 3. The reduction of input resistance is mainly due to inhibitory synaptic inputs. Independent variation of average excitatory (A) and inhibitory (B) conductances in the same cell. The cell was initially tuned to yield about 80% reduction of input resistance (Gi_0=75.2 nS, Ge_0=15.2 nS). Gi_0 and Ge_0 variations are plotted with respect to these standard values (labeled 100%). The percent reduction of input resistance (R_{in}) from the control condition, without point conductance-clamp (321 MΩ), to the input resistance with point conductance-clamp depended linearly on Gi_0, but did not depend on variations in Ge_0. Four independent measurements in the standard conditions (labeled 100%) were performed at different times during the experiment to estimate the variability of the resistance estimation procedure. C: Group data for five pyramidal cells. Ge_0 and Gi_0 are initially tuned to yield a reduction of 75%. Gi_0 is then varied. The reduction in input resistance depended linearly on Gi_0 (slope of the linear fit: 258%/μS). All points were calculated on the basis of an average of five hyperpolarizing pulses (20–140 pA) each repeated five times. D: dependence of input resistance on Ge_0 and Gi_0 in the point conductance model (see Experimental Procedures and Fig. 5B).

solution of 4% paraformaldehyde. Sections were then washed 20 min with 1% H_2O_2 to eliminate endogenous peroxidase. Slices were repeatedly (4×5 min) washed in a phosphate-buffered saline containing 2.5% dimethyl sulfoxide. Following 2 h incubation in avidin biotin complex (ABC kit; Vector Laboratories, Burlingame, CA, USA), the peroxidase product was revealed using tetramethylbenzidine using the following procedure. Slices were incubated for 20 min in a phosphate buffer solution (0.1 M; pH 6.0) containing 0.4% ammonium chloride and 0.001% tetramethylbenzidine. This reaction was stabilized by incubating the tissue for 15 min in a phosphate buffer containing 0.4% NH_4Cl, 1% cobalt chloride, 0.1% diaminobenzidine and 0.05% H_2O_2. Slices were then mounted and dried for tracing using a Neurolucida system (Microbrightfield Inc., Colchester, VT, USA).

Data acquisition

Data were acquired using two computers. The first computer was used for standard data acquisition and current injection. Programs were written using Labview 6.1 (National Instrument), and data were acquired with a PCI16-E1 data acquisition board (National Instrument). Data acquisition rate was either 10 or 20 kHz. The second computer was dedicated to dynamic clamp (Fig. 1B). Programs were written using either a Labview RT 5.1 (National Instrument) or a Dapview (Microstar Laboratory, Bellevue, WA, USA) front-end and a language C backend. Dynamic clamp (Sharp et al., 1993; Hughes et al., 1998; Jaeger and Bower, 1999) was implemented using a PCI-7030 board (National Instrument) at a rate of 1.2 kHz, or a DAP-5216a board (Microstar Laboratory) at a rate of 10 kHz. Dynamic clamp was achieved by implementing a rapid (0.83 ms or 0.1 ms) acquisition/injection loop in current clamp mode. There was no difference between the two experimental setups; therefore, all data were pooled. All experiments were carried in accordance with animal protocols approved by the N.I.H. Efforts were made to minimize the number of animals used and their suffering. A total of 33 pyramidal cells were used in this study.

Data analysis

Fitting procedures were based on the Nelder-Mead minimization method with a tolerance of 1% (Nelder and Mead, 1965). To have a good estimate of the coefficient of variation, the histograms of inter-spike intervals (ISIs) were fitted by a gamma distribution (Fig.

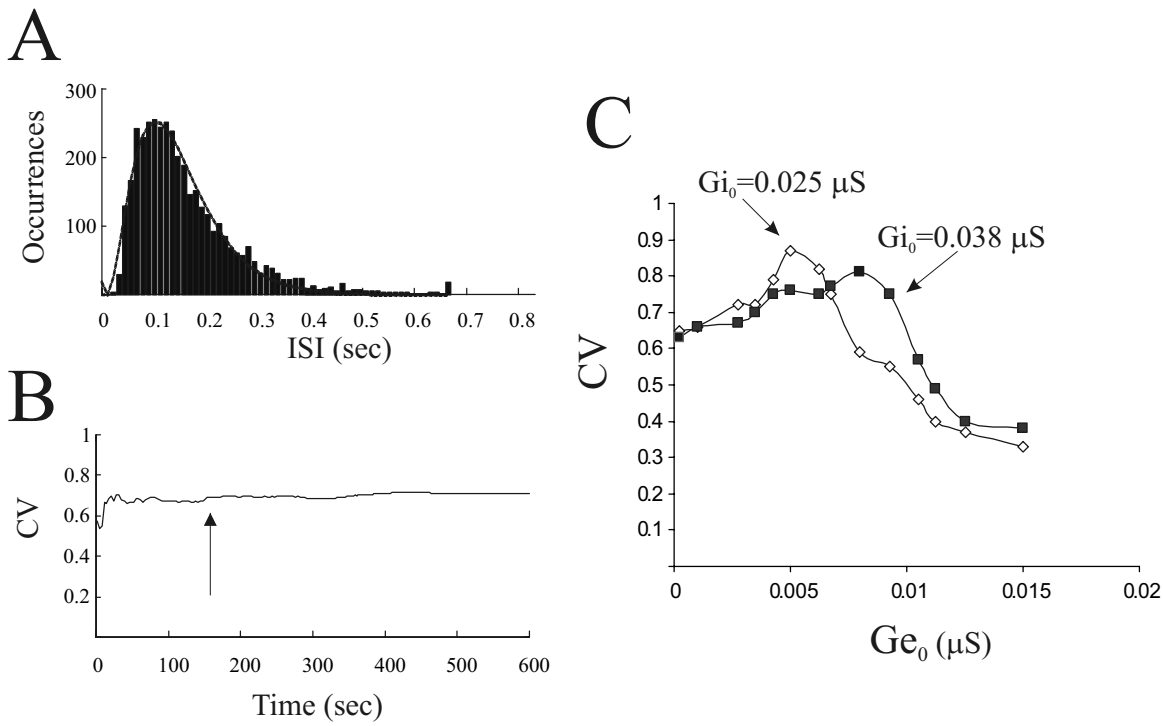

Fig. 4. Interspike intervals are Poisson-distributed and highly variable. A: The distribution of ISIs (bars; 10 ms bins) was well approximated by a Poisson distribution (curve; γ distribution; coefficient $r=1.8$). ISIs were computed on the basis of 4000 spikes recorded during 660 s (6 Hz spontaneous firing rate). Panel B shows that the CV becomes stable after about 150 s (arrow; 900 spikes; final value 0.7; $Ge_0=6.3$ nS, $Gi_0=9.3$ nS, $\sigma_e=7.5$ nS, $\sigma_i=19$ nS). C: Dependence of CV on Ge_0 for two fixed values of the mean inhibitory conductance ($\sigma_e=7.5$ nS, $\sigma_i=19$ nS). The CV depended on the average level of excitatory conductance (Ge_0) and was above 0.6 for a broad range of mean conductances (not shown). The highest values were obtained when Gi_0 was about four to five times larger than Ge_0. Two examples for the same cell are shown for two values of Gi_0.

4A) of the form:

$$P(t)=\frac{(\mu r)^r(t-\tau_d)^{r-1}e^{-\mu r(t-\tau_d)}}{\Gamma(r)} \text{ for } t>\tau_d$$

where μ, τ_d and r were free parameters such that $\mu=1/(<ISI>-\tau_d)$, $r=1/(\sigma_{ISI}\ \mu)^2$ $\tau_d>0$ was the 'dead time, and $\Gamma(r)$ is the gamma function.' For a Poisson distribution $r=1$. Across all conditions, the binning of the histograms of the ISIs remained fixed at 100, and the highest bin was six times the mean ISI. We found that these values ensured a good fit, irrespective of average firing rate and experimental variability. The coefficient of variation (CV) was calculated using the values of the fit:

$$CV=\frac{1}{\sqrt{r}(1+\tau_d\mu)}$$

Spike probability was computed as the ratio n/n_t, where n is the number of spikes elicited during the stimuli and 5 ms after the stimuli offsets, and n_t was the total number of spikes recorded.

For Figs. 7 and 8, the amplitudes of the input were expressed in units of the S.D. of the background noise (labeled 'signal-to-noise ratio,' or SNR), so that an amplitude of 1 corresponded to the case where the S.D. of the fluctuations during an input transient and before the transient were identical. When no background noise was included, the amplitudes of the signal current pulses were represented in the units of the S.D. of the noisy case, so that an amplitude of 1 corresponded to the S.D. of the background current injected in the noisy condition when no inputs were present.

Data were analyzed offline using MATLAB (The Mathworks, Natick, MA, USA).

Results are given as mean±S.D.

Computational modeling

Computational simulations were performed using two morphologically reconstructed models of cortical neurons. Simulations were performed based on a cat neocortical pyramidal layer 6 neuron from parietal cortex extensively studied and tuned to experimental data (total membrane area 34,636 μm^2; details in Contreras et al., 1996), and a rat prefrontal cortex layer 5 pyramidal cell obtained for the purpose of this study (total membrane area 28,642 μm^2; Fig. 5A, inset). This cell was recorded using the patch clamp technique while synaptic transmission was blocked. The resting membrane potential was −81 mV. The cell input resistance was 185 MΩ and was computed as the slope of the V-I curve obtained from a series of hyperpolarizing pulses of different amplitudes. The cell time constant was 37±5 ms and was obtained using the fit with a double exponential of the voltage drop elicited by 6 hyperpolarizing pulses of varying amplitude, repeated at least three times.

For the cat cell, passive model parameters were adjusted to fit intracellular recordings obtained after application of TTX and synaptic blockers (Destexhe and Paré, 1999) and they were kept constant over all simulations. An axial resistivity of $R_a=250$ Ωcm, membrane resistivity of $R_m=22$ kΩcm^2 ($R_m=50$ kΩcm^2 in the axon), and capacitance of $C_m=1$ μF/cm^2 ($C_m=0.04$ μF/cm^2 in the axon) were used, where C_m was increased and R_m were decreased by a factor of 1.45 to account for the surface correction due to dendritic spines (DeFelipe and Fariñas, 1992). R_a and R_m for the rat cell were fitted to results obtained from hyperpolarizing current injection *in vitro*, and were $R_a=50$ Ωcm and $R_m=67$

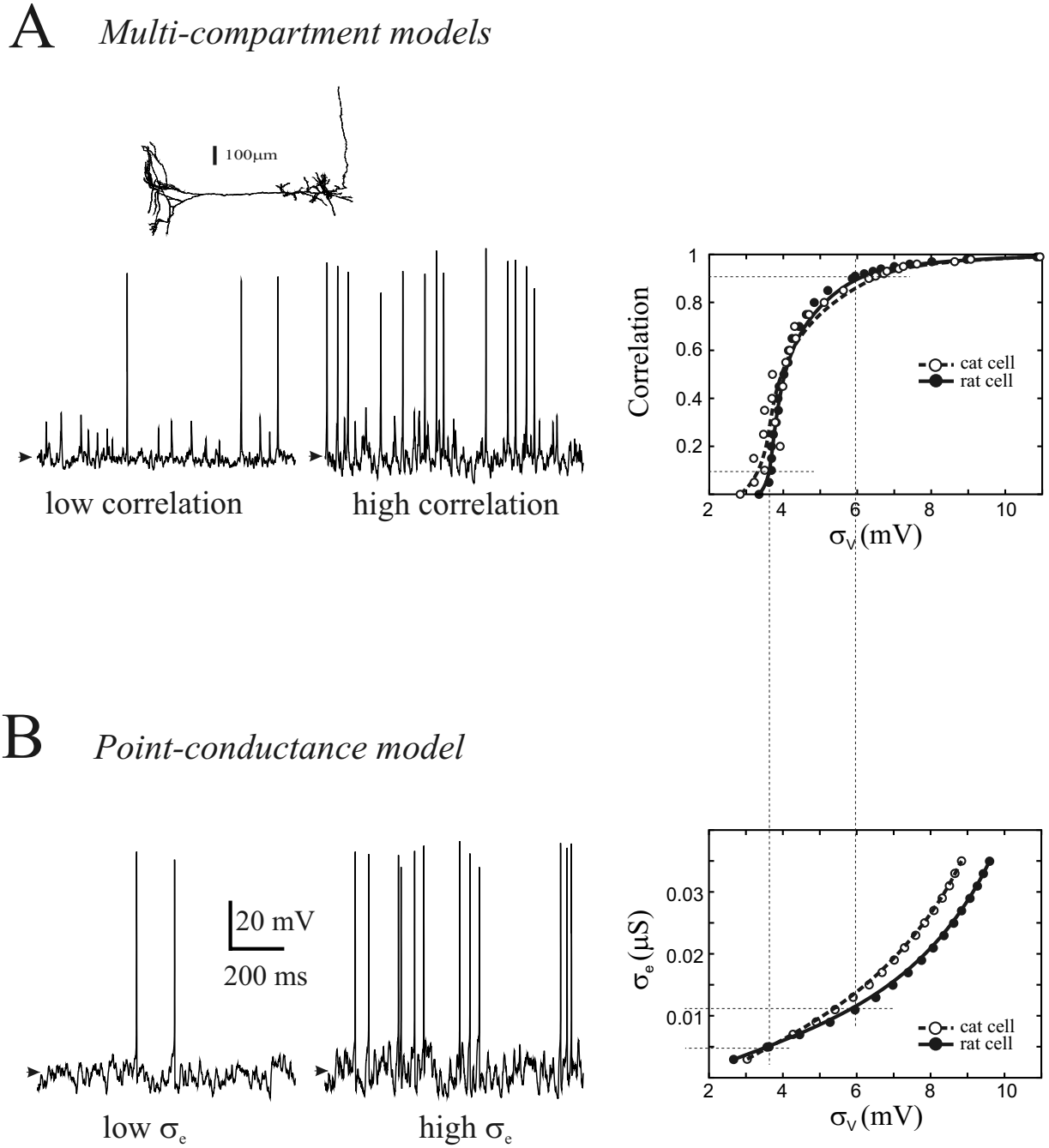

Fig. 5. Relationship between variance and correlation of synaptic inputs. A: Detailed model: The left panels show sample voltage traces for low (c=0.1; average membrane potential −65.5 mV; arrow) and high (c=0.9; average membrane potential −65.2 mV; arrow) AMPA synaptic correlations. The right panel shows the relationship between the amount of synaptic correlations and the resulting S.D. of the membrane voltage. Horizontal dashed lines correspond to the sample traces shown on the left. The correlation among inhibitory synapses was fixed (c=0). The inset shows the detailed morphology of the rat cell used in this study. B: Point conductance model: The left panels show sample voltage traces for low (σ_e=5 nS; average membrane potential −64.8 mV; arrow) and high (σ_e=11 nS; average membrane potential −64.9 mV; arrow) S.D. of the stochastic variable σ_e representing excitatory inputs to the one compartment model. The right panel shows the relationship between σ_e and the resulting S.D. of the membrane voltage of the point-conductance model. The dashed lines show that there is a one-to-one correspondence between a value of the correlation and a σ_e. The S.D. of the stochastic variable representing inhibitory inputs was fixed (σ_i=15 nS). The dashed lines correspond to the sample traces shown on the left. Low (5 nS) and high (11 nS) σ_e yield membrane potential fluctuations and firing rate equivalent to correlations those obtained in the detailed model for synaptic correlations c=0.1 and c=0.9 respectively.

kΩcm^2 (R_m=50 kΩcm^2 in the axon). The same values for spine correction and capacitance were used as in the case of the cat cell.

Voltage-dependent conductances were inserted in the soma, dendrites and the axon of each reconstructed cell to simulate active currents (sodium current I_{Na}, delayed-rectifier potassium

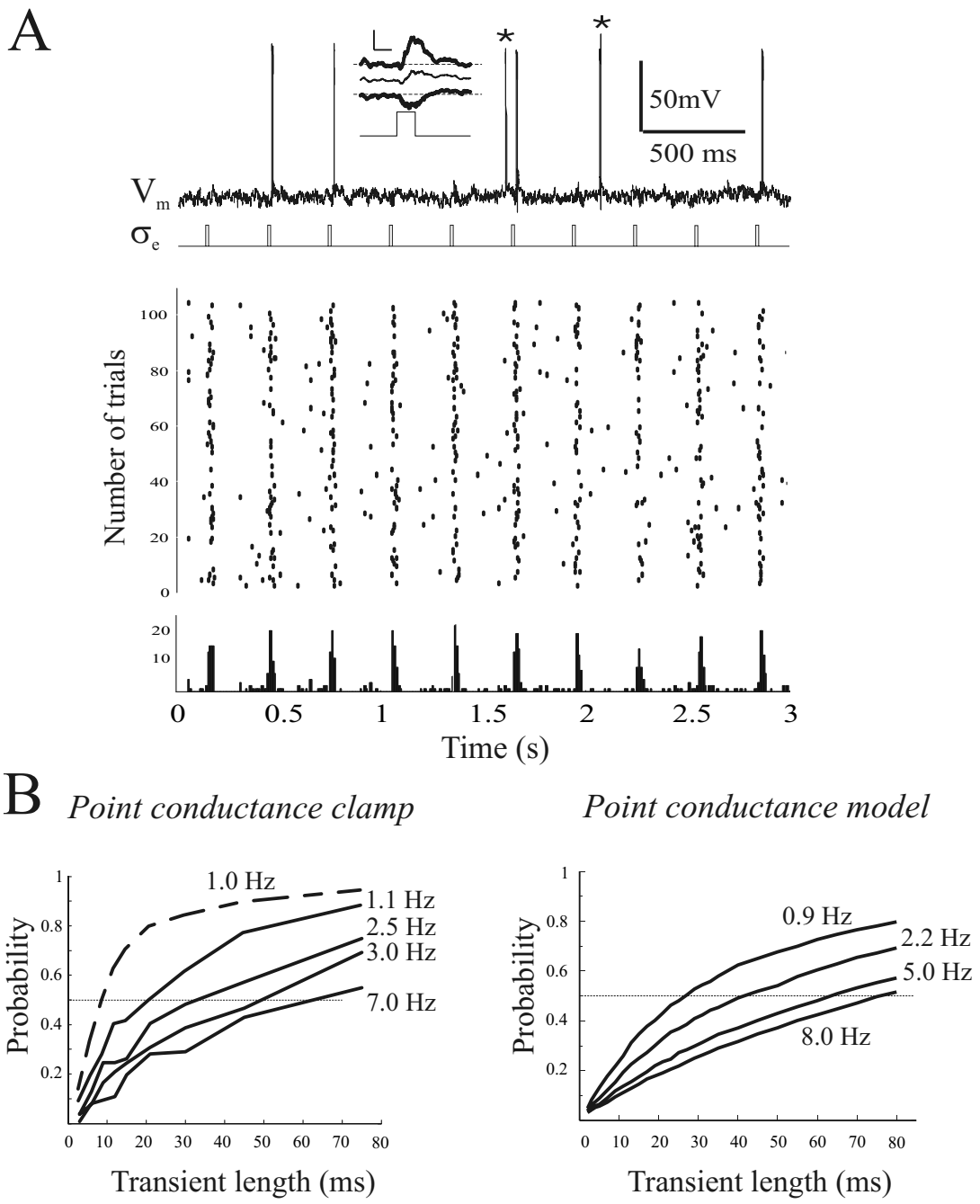

Fig. 6. Detection of transient changes in the variance of synaptic inputs. A: A pyramidal cell was injected with background synaptic noise (Ge_0=5 nS, Gi_0=25 nS, σ_e=5 nS, σ_i=12.5 nS). The S.D. of the excitatory and inhibitory stochastic variables was doubled for a duration of 30 ms (only σ_e is represented), mimicking the arrival of correlated synaptic inputs. The cell was able to detect this transient by emitting a spike time locked to the signal onset. Top: Sample trace showing two spontaneous spikes (*) and four evoked spikes. Note that the membrane potential of the cell was not significantly affected by the 10 stimuli. Middle: Spike rastergram with about 100 of 200 trials shown. Inset: The thin curve shows the average membrane potential computed around all transients, in all trials. The thick curves represent the S.D. of the membrane potential around the transient. Note that the average membrane potential during the transient stayed within the S.D. of the membrane noise (horizontal dashed lines). Inset scale bars=4 mV, 30 ms. Bottom: spike histogram (10 ms bins) of the rastergram above, showing clear peaks at the time of stimuli onset. The cell's average membrane potentials (actions potentials truncated at −50 mV) outside and inside the σ_e pulses were −68.1 mV (±3) and −67.1 mV (±4.2) respectively. B: Left: Signal detection capability (probability that an action potential indicated the presence of a transient input) for varying transient lengths. The dashed curve corresponds to the cell shown in panel A. Note that this cell is able to detect about 50% of 10 ms long stimuli. The cell had a spontaneous firing rate of about 1 Hz. The four other curves are from a different cell. Four different levels of spontaneous firing (1.1 Hz, 2.5 Hz, 3 Hz and 7 Hz corresponding to Ge_0 values of 10, 13, 17, 24 nS, Gi_0 fixed at 60 nS) are represented. Right: The point conductance model reproduces qualitatively the experimental data. Note that for low spontaneous firing rates, the detection capabilities of the cell depended non-linearly on transient lengths (model and experiments).

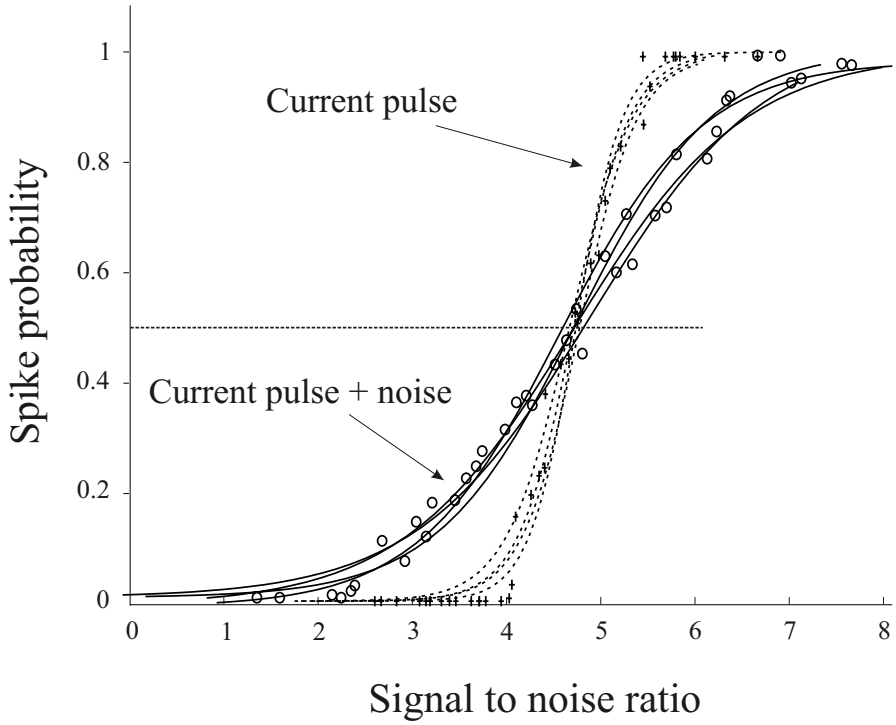

Fig. 7. Effect of simulated synaptic background noise on the detection of transient current pulse injections. The continuous curves show the sigmoid fits to the data points (circles) representing the spiking probability of a cell undergoing simulated synaptic noise (Ge_0=7 nS, Gi_0=26 nS, σ_e=2.5 nS, σ_i=7.5 nS, spontaneous firing 0.5 Hz) in response to 20 ms current pulses of increasing amplitudes. The cell was able to detect amplitudes as small as 2.8 times the S.D. of the current resulting from the injection of the synaptic noise. The firing probability was however smaller than 0.5. The dashed curves were obtained when the same cell did not receive simulated synaptic noise but was kept depolarized at the same average level as in the case with fluctuating synaptic noise (Ge_0=7 nS, Gi_0=26 nS, σ_e=0 nS, σ_i=0 nS, spontaneous firing 0 Hz, data points represented by crosses). Current pulses smaller than 4.5 times the S.D. of the current resulting from of the noise injected previously rarely succeeded in eliciting spiking. Above this value, the probability of spiking rapidly became 1. Each data point was obtained from 200 trials. Each curve was established on the basis of at least 10 data points. The experiment was repeated four times in each condition to assess the robustness of the data acquisition and analysis procedures.

current I_{Kd} and voltage-dependent potassium current I_M). All currents were described by Hodgkin-Huxley type models with kinetics taken from a model of hippocampal pyramidal cells (Traub and Miles, 1991), adjusted to match voltage-clamp data of cortical pyramidal cells (Huguenard et al., 1988). For the rat cell, maximal dendritic conductance densities of 44.8 mS/cm^2 (30.9 mS/cm^2 in soma, 309 mS/cm^2 in axon) for I_{Na}, 8.6 mS/cm^2 (6 mS/cm^2 in soma, 60 mS/cm^2 in axon) for I_{Kd}, and 0.43 mS/cm^2 (0.3 mS/cm^2 in soma) for I_M (no I_M in axon) were used. Slightly larger values of 52.3 mS/cm^2 (36.1 mS/cm^2 in soma, 361 mS/cm^2 in the axon) for I_{Na}, 10.1 mS/cm^2 (7 mS/cm^2 in soma, 70 mS/cm^2 in axon) for I_{Kd}, and 0.51 mS/cm^2 (0.35 mS/cm^2 in soma) for I_M (no I_M in the axon) were used for the cat cell.

Synaptic currents were incorporated using two-state kinetic models of glutamate α-amino-3-hydroxy-5-methyl-4-isoxazolepropionic acid (AMPA) and $GABA_A$ receptor types (Destexhe et al., 1994) with quantal conductances of 869 pS for distal regions, 600 pS for proximal region for AMPA and 1739 pS for $GABA_A$. The contribution of NMDA receptors was assessed in control experiments. In a few simulations NMDA currents were included along with AMPA currents (see Results). No metabotropic receptors were included. For both cells, the densities of synapses in different regions were estimated from morphological studies of neocortical pyramidal cells (White, 1989; Larkman, 1991; DeFelipe and Fariñas, 1992; e.g. 16,563 glutamatergic- and 3376 GABAergic-simulated synapses for the cat cell). An accelerating algorithm (Lytton, 1996) was used to perform the simulations in a time-efficient manner.

Synaptic background activity was explicitly simulated by the random activity of inhibitory and excitatory synapses according to Poisson processes with average rates of 5.5 Hz for $GABA_A$ synapses, and 1.0 Hz for AMPA synapses. These firing rates were chosen to account for the average low probability of release at excitatory synapses and were estimated from intracellular recordings of pyramidal neurons before and after application of TTX (Paré et al., 1998; Destexhe and Paré, 1999). The statistics of the synaptic background activity was modified by introducing a correlation in the random background activity. To accomplish this, we introduced some redundancy in the release events, without changing the mean release rate at single terminals (and therefore without change in the overall synaptic conductance). N_0 independent Poisson-distributed streams of release events were redistributed among all N synapses, which for $N_0<N$ led to a co-release of several synapses, whereas the release at each terminal still followed a Poisson process (see details in (Destexhe and Paré, 1999; Rudolph and Destexhe, 2001). A correlation of 0 was obtained when $N_0=N$, and a correlation of 1 for $N_0=1$ (Destexhe and Paré, 1999; Rudolph and Destexhe, 2001).

Current injections resembled the protocol used in the experimental setup, and consisted of a 3 s current pulse from which F-I curves were obtained. The un-normalized F-I curves were fit to a sigmoid of the form:

$$Y=\frac{a+be^{-cX}}{1+de^{-cX}}-\frac{b}{d}$$

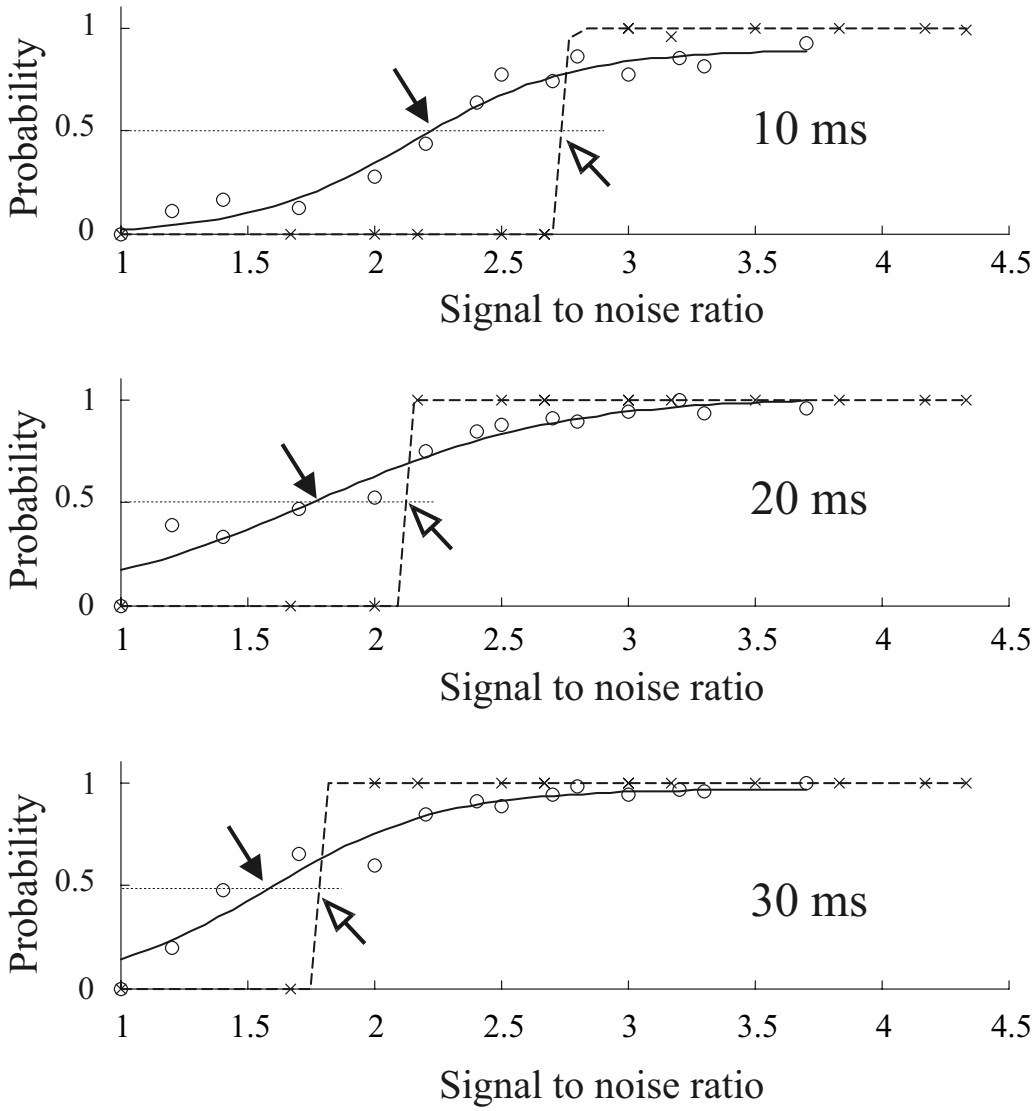

Fig. 8. Enhancement of correlation detection by background synaptic noise. Probability that an action potential indicated the presence of a transient input of 10 ms (top), 20 ms (middle) or 30 ms (bottom) as a function of the amplitude of the input. In all panels, open symbols represent experiments with synaptic background noise (Ge_0=14 nS, Gi_0=22.5 nS, σ_e=5 nS, σ_i=12.5 nS). In these experiments, inputs consist in a short (10 ms, 20 ms or 30 ms) increase in the S.D. of the background noise. In this condition, the spontaneous firing rate was about 1 Hz. Crosses represent experiments without synaptic background noise. In these experiments, the cell was depolarized to a resting level equivalent to the mean membrane potential with point-conductance clamp, and inputs consisted in short (10 ms, 20 ms or 30 ms) current pulses of varying amplitude. In this condition, the cell did not have a spontaneous firing rate. The curves are sigmoid fits of the data points. Each point is computed from 120 trials. In the case where synaptic background noise was included, the detection of the input signal ($P>0.5$; dashed lines) occurred for inputs amplitudes smaller than when no synaptic background noise was included (filled arrows and opened arrows respectively).

where the "working point" is defined as the stimulus amplitude corresponding to 50% of the maximal asymptotic firing rate, and the "gain" is defined as the maximum slope.

All simulations were performed using the NEURON simulation program (Hines and Carnevale, 1997), running on Dell computers (Dell Computer Corporation, Round Rock, TX, USA) under the LINUX operating system.

Point conductance model

A simplified model of synaptic background activity was incorporated into one-compartment models with membrane area, passive settings and voltage-dependent currents I_{Na}, I_{Kd} and I_M appropriate for the cat and rat pyramidal cells.

The synaptic background activity was simulated as a *fluctuating point conductance*, as previously described (Destexhe et al., 2001). The total synaptic current injected in dynamic clamp was calculated as the sum of two independent conductances

$$I_{syn}(t) = Ge(t)(V(t) - E_{AMPA}) + Gi(t)(V(t) - E_{GABA})$$

where E_{AMPA} and E_{GABA} are the reversal potentials for AMPA and $GABA_A$ conductances (0 mV and −75 mV respectively), and V is the instantaneous membrane voltage of the recorded pyramidal cell. The fluctuating conductances Ge and Gi are given by two OU processes (Uhlenbeck and Ornstein, 1930):

$$\frac{dGe(t)}{dt} = -\frac{1}{\tau_e}[Ge(t) - Ge_0] + \sqrt{D_e}\chi_1(t)$$

$$\frac{dGi(t)}{dt} = -\frac{1}{\tau_i}[Gi(t) - Gi_0] + \sqrt{D_i}\chi_2(t)$$

where Ge_0 and Gi_0 are average conductances, and τ_e and τ_i are time constants (2.7 ms and 10.7 ms respectively throughout this study), $\chi_1(t)$ and $\chi_2(t)$ are Gaussian white noise terms of unit S.D., D_e and D_i are the "diffusion" coefficients, and Ge and Gi are Gaussian variables with S.D.s $\sigma_e = \sqrt{D_e\tau_e/2}$ and $\sigma_i = \sqrt{D_i\tau_i/2}$ respectively. The procedure used for numerical integration of these stochastic equations is detailed elsewhere (Destexhe et al., 2001).

This formulation allows for an analytical expression of the power spectral characteristics of Ge and Gi (Gillespie, 1996). In previous work we showed that σ_e, σ_i, Ge_0 and Gi_0 can be tuned to match the S.D. and power spectral characteristics of the overall excitatory and inhibitory synaptic conductances measured at the soma of a reconstructed cat pyramidal cell undergoing random synaptic inputs (Destexhe et al., 2001). This study showed that, irrespective of the cell morphology, best fits were obtained for $Gi_0 \approx 5Ge_0$ and $\sigma_i \approx 2.5\sigma_e$. Unless otherwise noted, σ_e, σ_i, Ge_0 and Gi_0 will follow these constraints. Intracellular recordings during periods of intense network activity revealed an average V_m of about −65 mV when IPSPs reverse around −75 mV, and of about −51 mV when IPSPs reverse at −55 mV, as obtained with chloride-filled sharp electrodes (Destexhe and Paré, 1999). These values imply that chloride-mediated events (presumably $GABA_A$ conductances) dominate the overall conductance due to network activity.

Simulations of the point conductance model were performed with NEURON, and Visual C++ (Microsoft) was used to program the dynamic-clamp current injections from Labview RT, or Dapview.

RESULTS

Recreation of *in vivo*-like activity

Intracellularly recorded (n=5) layer 5 pyramidal cells of rat prefrontal cortex *in vivo* under urethane anesthesia exhibit large fluctuations in their membrane potentials, accompanied by occasional spontaneous discharges (Fig. 1A). These membrane fluctuations had a S.D. of about 4 mV (3.9±0.5 mV; n=4), the average membrane potential was around −65 mV (−65±2.6 mV; n=4), and the spontaneous discharge rate was highly irregular with a CV around 1 (0.94±0.17; n=4) and an average firing rate of about 4 Hz (3.7±1.5 Hz; n=4). The input resistances of these cells were around 40 MΩ (44±14 MΩ; n=5) and were low compared with *in vitro* recordings. These characteristics obtained under urethane anesthesia in rat prefrontal cortex were similar to those obtained in cat parietal cortex *in vivo* under ketamine-xylazine anesthesia (Paré et al., 1998; Destexhe and Paré, 1999).

In contrast, the slice preparation of rat prefrontal cortex showed little spontaneous activity. Intracellularly recorded layer 5 pyramidal neurons (n=21) in this *in vitro* preparation had no spontaneous firing, and their membrane potentials were almost constant around a resting value of −82±3 mV (n=21), as shown for the cell in Fig. 1B1. We attempted to mimic *in vivo* conditions *in vitro* using a stochastic model of background synaptic activity, implemented by the real-time injection of a fluctuating conductance (Fig. 1B, left) obtained as the sum of two random processes with time constants given by AMPA (2.7 ms) and $GABA_A$ (10.7 ms) postsynaptic conductances variation (see Experimental Procedures). Fig. 1B3 shows the current resulting from the injection of these two fluctuating conductances, and Fig. 1B2 shows the corresponding membrane potential. Fig. 1C shows a free running bout of activity of a prefrontal cortex cell *in vitro* undergoing simulated synaptic background activity. With the proper parameter tuning, this cell mimicked the measurements of background activity obtained *in vivo* (Fig. 1A; Paré et al., 1998; Destexhe and Paré, 1999): It had a low input resistance (41 MΩ), an average membrane potential of −65.8 mV (an estimated 10 mV junction potential was subtracted from the measured membrane potential; see Experimental Procedures), a S.D. for the membrane potential fluctuations of 4.6 mV, a CV of 0.91 and an average firing rate of 2.5 Hz. Because this cell was not bursting, its CV was slightly lower than that typically obtained from *in vivo* recordings (Holt et al., 1996). Also, the membrane potential *in vitro* contained more spectral power at high frequency than that obtained *in vivo*. The conductances were fit to the spectral characteristics of the excitatory and inhibitory somatic conductances measured on a reconstructed multicompartmental cell receiving a realistic distribution of 16,563 glutamatergic synapses and 3376 GABAergic synapses releasing in a Poisson fashion at 1 Hz and 5.5 Hz respectively (Destexhe et al., 2001). Additional simulations were conducted to assess the influence of NMDA receptors on input resistance and average depolarization level. In these simulations, NMDA receptors were paired with AMPA receptors, with an NMDA/AMPA conductance ratio that was varied between 0 and 0.5 (McAllister and Stevens, 2000; Watt et al., 2000). $GABA_A$ synapses were left unchanged. The simulations showed than the input resistance changed by less than 5% and V_m changed by less than 4% in comparison with the model where only AMPA and $GABA_A$ receptors were included (not shown). These results show that a judicious choice of the first two moments (mean and S.D.) of synaptic background activity for excitation and inhibition (captured here by two OU processes) are sufficient to capture essential *in vivo* characteristics *in vitro*.

The input resistance of a cell determines how much current will be required to bring it to threshold, and hence the minimum synaptic input needed to elicit a spike. We attempted to reproduce the five-fold increase in input resistance observed *in vivo* when background activity was suppressed by TTX (Paré et al., 1998; Destexhe and Paré, 1999). We first tried to mimic these *in vivo* conditions by using a large stimulating electrode to stimulate the afferents to a pyramidal cell recorded intracellularly *in vitro* (Fig. 1B, right panel). The stimulation patterns were Poisson trains (120 Hz and 200 Hz) of pulses of variable amplitude (Fig. 2A, lower trace). During the synaptic stimulation, negative pulses of different amplitudes were somatically injected (time t_1 in Fig. 2A), and the input resistance was computed as the slope of the resulting I-V curve. Fig. 2B shows that the average membrane potential only increased by about 9 mV in this cell, while the input resis-

tance decreased only by a factor of 1.25. Changing the extracellular stimulation strength and frequency was unsuccessful in generating more than a 1.5-fold decrease of input resistance (1.4 ± 0.3; $n=5$).

In contrast to the results of extracellular stimulation, the simulation of synaptic activity using the point-conductance clamp depolarized the cell by about 16 mV and decreased its input resistance by a factor of 4.4, closer to what would be observed *in vivo* (Fig. 2C). The point conductance clamp was constrained by four main parameters: The average excitatory Ge_0 and inhibitory Gi_0 conductances, and their S.D.s σ_e and σ_i respectively (see Experimental Procedures). A systematic variation of these parameters revealed that the reduction of input resistance was mainly due to the mean level of inhibitory conductance Gi_0 (Fig. 3A and B). The relationship between the reduction in input resistance and average inhibitory conductance was linear (Fig. 3C) with an increase in the mean inhibitory conductance yielding a proportional decrease in input resistance (slope: 260%/μS). The point-conductance model reproduced well these experimental findings (Fig. 3D), and further explained why such a reduction in input resistance occurred; As Gi_0 was increased, the membrane potential became dynamically 'clamped' to the reversal potential of GABA (−75 mV), and any voltage deflection produced by a current pulse was apparently reduced, if it tended to push the membrane potential away from −75 mV. Because the absolute values for Gi_0 were about four times greater than for Ge_0 (from the rest, about −60 mV, the differential to the GABA reversal (15 mV) is four times smaller than the voltage differential to the AMPA reversal potential (60 mV)), it follows that Rin should be more sensitive to Gi_0 variation than to Ge_0 variations. In general, this sensitivity should not be strictly linear because it depends on the voltage dependence of the currents active at rest. However, Fig. 3 shows that the linear approximation gave a good fit. Changes in the S.D. of excitatory and inhibitory inputs introduced no significant change in input resistance (not shown).

Firing variability

The spontaneous firing pattern of cells recorded in the point-conductance model were highly irregular. The ISI histogram had the shape of a γ distribution (Fig. 4A). The best fits of the ISI distribution with a γ function yielded low r coefficients (see Experimental Procedures; 2.2 ± 0.5; $n=7$), indicating that the ISI distribution approximated a Poisson process with refractory period. A measure of the spiking irregularity was given by computing the CV of the ISIs, defined as the ratio of the S.D. of the ISIs to its mean. For the cell shown in Fig. 4B, the CV reached a steady state value (less than 3% variation per 20 s) of about 0.7 after about 150 s. The CV depended on the mean excitatory conductance Ge_0 (Fig. 4C). In this cell, the CV was maximal for Gi_0 to Ge_0 ratios between 4 and 5 (4.3 ± 1.1; $n=4$ with maximum average CV of 0.83 ± 0.04). For high Gi_0/Ge_0 ratios the cell had a low firing rate (about 1 Hz for $Ge_0=0.0025$ μS) and large regular ISIs. This regularity at low frequencies may be due to a slow inactivation of a spike-induced potassium current (such as a slow calcium-dependent I_{AHP} or slowly inactivating potassium currents). Further pharmacological studies would be required to better characterize these currents. For low ratios, the cell tended to fire at higher rates (19 Hz for $Ge_0=0.011$ μS) with a low CV that was obtained when the CV vs. time curve reached a stable state (less than 3% variation per 20 s). CV_2 yielded qualitatively the same result because there was no significant modulation of the firing rate during the data collection (Holt et al., 1996). Since the excitatory driving force is about four to five times larger than the inhibitory driving force, these results indicate that the firing variability is maximal (CV highest) in conditions where the excitatory and inhibitory currents are about equal, in other words when excitatory and inhibitory inputs are balanced (Shadlen and Newsome, 1994; Troyer and Miller, 1997).

These results provided a basis for the choice of the values of the parameters of the two OU processes that describe synaptic background activity. σ_e was set to yield an appropriate level of membrane fluctuations (about 4 mV; typical values range between 3 and 10 nS), Ge_0 was set to yield an appropriate level of average depolarization and background firing (15 mV depolarization and 5–10 Hz respectively; typical values range between 5 and 15 nS), and the value of Gi_0 was the primary determinant of the input resistance of the cell (about 50 MΩ; typical values range between 25 and 70 nS). σ_i Remained a free variable that could be used to set the gain of the cell (see below; typical values range between 7 and 25 nS). Note that the manipulation of σ_e to adjust membrane potential fluctuations may also have consequences for the firing rate of the cell.Ge_0did not affect the membrane fluctuation, so σ_e should be set first. The exact values for these four parameters are set in accordance to the intrinsic passive properties of the particular cell being recorded.

Variance detection

Input signals consisting in the simultaneous firing of a population of cells occur *in vivo* on a background of random synaptic noise. In order to assess how correlated synaptic events are reflected at the soma, we use a reconstructed multi-compartmental cell (Fig. 5A) from the rat prefrontal cortex that received 16,563 AMPA synapses and 3376 GABA synapses discharging in a Poisson manner at 1 Hz and 5.5 Hz respectively (Destexhe and Paré, 1999). At the soma, these synaptic inputs yielded voltage fluctuations that depended on the amount of correlations introduced among the synaptic inputs. Fig. 5A shows sample traces in cases of low (0.1) and high (0.9) correlations in the excitatory synaptic inputs, and the relationship between the S.D. of the membrane potential measured at the soma and the synaptic correlation (right panel). Fig. 5B shows that for the point-conductance model (one compartment) it was possible to find a unique value of the S.D. σ_e of the stochastic variable Ge that resulted in a simulated somatic synaptic current that yielded membrane voltage fluctuations equivalent to the ones of the detailed model. For comparison, we also show the curves obtained with the reconstructed model of a cat pyramidal cell extensively

used in other studies, and for which parameters have been directly constrained by *in vivo* recordings (Destexhe and Paré, 1999). There were no significant differences between the two reconstructed cells.

In previous models (Rudolph and Destexhe, 2001) of pyramidal neurons, transient correlation changes down to 2 ms duration could be detected. As shown here (Fig. 5) and previously (Destexhe et al., 2001), the correlation of synaptic inputs translates into the variance of synaptic conductances. Together these results predict that cortical neurons should be able to detect brief changes in the variance of synaptic conductance. To test this prediction, we assessed the ability of cells recorded *in vitro* to detect transient changes in the variance of their background synaptic conductances. Fig. 6 shows an example of a cell that received continuous simulated noise (Ge_0=5 nS, Gi_0=25 nS, σ_e=5 nS, σ_i=12.5 nS). Under these conditions, the cell fired spontaneously at less than 1 Hz, and its membrane potential fluctuated around −68 mV±3.6 mV. At predetermined times, the S.D. of the noise (both σ_e and σ_i) was doubled for 30 ms every 330 ms, mimicking a 3 Hz signal consisting of synchronous inhibitory and excitatory inputs. The inset of panel A shows the average membrane potential and S.D. around such a pulse, across all the trials. The average membrane potential during the signal increased, but remained smaller than the S.D. of the membrane potential before or after the signal (horizontal dashed lines). The cell, however, fired preferentially during these 30 ms transients, as indicated by the firing histogram across about 100 trials (Fig. 6A). The cell was able to detect events that were as short as 10 ms (Fig. 6B-left, dashed curve), a time scale much shorter than the cells' typical membrane time constant (about 30 ms). The probability that a spike was elicited in response to a transient depended on the spontaneous firing rate of the cell. Fig. 6B-left shows the probability as a function of signal length, for four different spontaneous firing rates, in a different cell (continuous curves). The shortest signals this cell was able to detect (probability >0.5) ranged from 20 ms to 65 ms as its background firing-rate increased from 2 Hz to about 7 Hz (more than twice the frequency of the signal). As the background firing rate increased, the probability for the input signal to arrive within the relative refractory period of the cell increased, and the probability of spiking in response to the signal therefore decreased. This might explain why the same signal is better detected with low background firing. An accurate model of the biophysical properties of prefrontal regular spiking cells would be warranted to assess the relative refractory period of these cells and its dependence on various intrinsic currents. Unfortunately, sufficient information on intrinsic currents is not yet available for these cells. Note that for low firing rates (<7 Hz), the detection probability was non-linear. As the spontaneous firing of the cell increased, the probability of detecting a spike belonging to the signal became proportional to the signal length. Qualitatively similar results were obtained in eight other cells. The point conductance model reproduced this finding (Fig. 6B right).

Fig. 7 shows the probability of spiking of a cell that received somatically injected current pulses of fixed duration (20 ms) and varying amplitude. In a first series of experiments, the cell did not receive simulated background synaptic activity. In this condition, its response was all-or-none (dashed curves) marking the presence of a current threshold below which signals were not detected, and above which signals were always detected. This protocol was repeated in the presence of simulated synaptic noise (Ge_0=7 nS, Gi_0=26 nS, σ_e=2.5 nS, σ_i=7.5 nS, same somatic current pulses as above). The slope of the response curve changed, indicating that the cell was able to partially detect signals that were below the 'classical' threshold. However, the detection probability remained smaller than 0.5. At P=0.5, the ratio of the slopes in the noise case to the no-noise case was 0.51±0.25 (n=6 cells; 19 curves with pulse widths of 10, 20 or 30 ms). Note that the absolute values for the mean and S.D. of excitatory and inhibitory conductance differed slightly from cell to cell, due to their difference in input resistance and threshold. These values were tuned for each cell to simultaneously achieve the desired depolarization (approximately −60 mV, spontaneous rate <3 Hz), membrane potential fluctuations (S.D. approximately 4 mV), and input resistance (approximately four times smaller than without noise).

The variance transients are completely determined by their duration and amplitude. Fig. 8 shows the sensitivity of the cell to several transient increases in σ_e and σ_i of various amplitude for durations of 10 ms, 20 ms and 30 ms. In these experiments, Gi_0 was set to yield a low input resistance (Gi_0=22.5 nS; Rin=36.3 MΩ; Fig. 3C). Since variations in mean excitatory input did not change the cell input resistance significantly (Fig. 3A), Ge_0 was an independent parameter that could be used to set the spontaneous firing rate of the cell. Ge_0 was adjusted to obtain a low spontaneous firing rate (0.9 Hz; Ge_0=14 nS), σ_e was set to yield about 4 mV fluctuations in the membrane potential (σ_e=5 nS), and σ_i was set to 2.5×σ_e in accordance with previous simulation studies (Destexhe et al., 2001). In the presence of this noise, the cell was able to detect transient variance changes of 10 ms duration and of amplitude equal to about 1.5 times the S.D. of its noisy excitatory inputs, while it was above chance for inputs as small as 2.2 times the SNR (filled arrow). Without the simulated synaptic background noise but with the cell depolarized to the same level as with background synaptic noise (−62 mV), its ability of detecting current steps of 10 ms durations and varying input amplitude adopted an all-or-none step profile (dashed curves). The SNR for detection corresponded to about 2.7 times the S.D. of the previously injected noise (open arrows). As the duration of the signal increased, the threshold for detection decreased. In all cases, the cell was more sensitive to its input if it was injected with simulated synaptic background noise (filled arrows are always to the left of the open arrows). The points where P>0.5 in the noisy cases were 1.47 (±0.4, n=8), 0.98 (±0.25, n=8), 0.65 (±0.14, n=8) lower than the corresponding points of the all-or-none curves for

pulses of 10, 20 and 30 ms, respectively (none were higher). Note that the relative difference in SNR between the two curves at $P=0.5$ is progressively reduced as the length of the transient is increased. These results indicate that the improvement in signal detection due to synaptic background noise decreases as the signal duration increases to about 40 ms (the approximate time constant of the cells' membrane). Very short transients (2 ms and 5 ms) were ineffective in eliciting spiking probabilities greater than 0.9 with σ_e transients smaller than six times the S.D. of the background noise (data not shown). For such values, the average membrane potential variation during the transient was typically greater than its average before the transient (unlike Fig. 6A inset).

The coding strategies of cortical cells are still largely unknown. The response to short signals such as described above may only be one way of detecting information. On longer time scales, other ways may include the modulation of the cell's firing rate (deCharms and Zador, 2000).

Gain modulation

In order to assess the ability of the cells to respond to sustained rather than transient increase in their input, we measured their responses to 3 s long current pulses injected at the soma. Fig. 9 shows the firing rate of a cell when the four parameters of the point conductance model were systematically varied. An increase in mean excitatory or inhibitory conductances resulted in a leftward (7.5 pA/nS) or rightward (2.8 pA/nS) shift of the F-I curve without any significant change to the gain of the cell (Fig. 9C and D). The maximal firing rate allowed by the cell given its adaptation currents (saturation) remained almost unaffected by changes in mean conductances. Increases in the S.D. of the simulated excitatory inputs resulted in a slight shift of the F-I curve upwards (0.6 Hz/nS), and an increase in the slope of the sigmoid fit (in Fig. 9A, with a 100 pA input, the gain of the cell increased by 3.2 Hz/pA per nS increase in σ_e). Increases in the S.D. of inhibitory inputs had two effects on the cell's F-I curve. The first was to increase its maximal firing rate for a given current pulse amplitude. The second was to increase the mid-height slope of the curve (In Fig. 9B, with a 100 pA input, this slope increased by 6.1 Hz/pA per nS increase in σ_i) compatible with other recent studies performed in constrained excitatory and inhibitory balanced conditions (Chance et al., 2002). The slope (also called gain) of the F-I curve taken at mid-height between the spontaneous firing rate, and the maximal firing rate is a measure of the sensitivity of the cell to its inputs. A low gain (slope) indicates that large inputs will be required to induce noticeable changes in firing rate; at high gain, small variations in the inputs will results in large variation in the cell's output firing rate. Note that for this cell, the increase in gain varied non-linearly with σ_i: a doubling in σ_i with $\sigma_i=2.5$ nS resulted in a smaller slope increase than a doubling of σ_i with $\sigma_i=9$ nS. Increases in S.D. of either the excitatory or inhibitory inputs had the same general effects on the maximal firing rate and slope. Because the mean inhibitory and excitatory conductances were kept constant, changing the variance of either synaptic input had little effect on the total synaptic conductance received by the cell, and on its input resistance (not shown). To assess the robustness of our measurements of slope and mid-point, we recorded from cells in stationary conditions (same Ge_0, Gi_0, σ_i and σ_e), and we repeatedly measured the F-I curve at regular intervals. The mid-point currents, and mid-point slopes of the F-I curve were obtained from the sigmoidal fits and were used to quantitatively assess the error in working point and slope estimation. The slope varied by less than 9%, and the midpoint varied by less than 8% (three cells, at least 15 curves each, data not shown).

Due to the length of the experiments required to obtain the curves displayed in Fig. 9, it was not possible to collect data for more than three or four values for each of the four parameters Ge_0, Gi_0, σ_e and σ_i of the stochastic model. In order to better assess the effects of these parameters on the gain of the cell, we studied the computational model placed in the same condition as in the experiments. These simulations showed that the working point of the cell was mainly determined by the balance of mean inhibition and excitation, and the S.D.s of excitatory and inhibitory inputs could individually modulate the gain (the slope range due to σ_e variations was 75–89 Hz/nA and was 72–92 Hz/nA for σ_i). Simulations performed with the same model, but using stimuli consisting of AMPA conductance changes (instead of current transients) yielded qualitatively similar results for the impact of the various parameters Ge_0, Gi_0, σ_e and σ_i (not shown). These simulation results were in qualitative agreement with the experimental findings of Fig. 9; the mean excitation and mean inhibition modulated the working point, and the excitatory and inhibitory variances modulated primarily the gain. Three currents (I_{Na}, I_{kd} and I_M) were therefore sufficient to capture the influence of synaptic background noise on the I-F curve observed experimentally.

DISCUSSION

Although the properties of neurons recorded *in vitro* are quite different from those recorded *in vivo*, they were much more similar when neurons *in vitro* were stimulated with two stochastic processes simulating excitatory and inhibitory conductances. We used the dynamic clamp technique to inject these conductances in layer 5 pyramidal cells of the rat prefrontal cortex. As a consequence, cells were depolarized by about 15 mV, their input resistances were decreased four-five-fold, and their membrane voltages fluctuated with a 4 mV S.D. They were able to produce action potentials at low rates (2–10 Hz) with a high coefficient of variation. We showed that the mean inhibitory input, but not the mean excitatory input, was a key determinant of the input resistance of the cell and that the coefficient of variation of the ISIs was maximal when the mean excitatory and mean inhibitory conductances had a ratio of 4–5. Using a detailed multi-compartmental model of a rat prefrontal cortex cell, we confirmed that the S.D. of the stochastic variable representing excitatory inputs could be interpreted as a level of correlation in presynaptic inputs

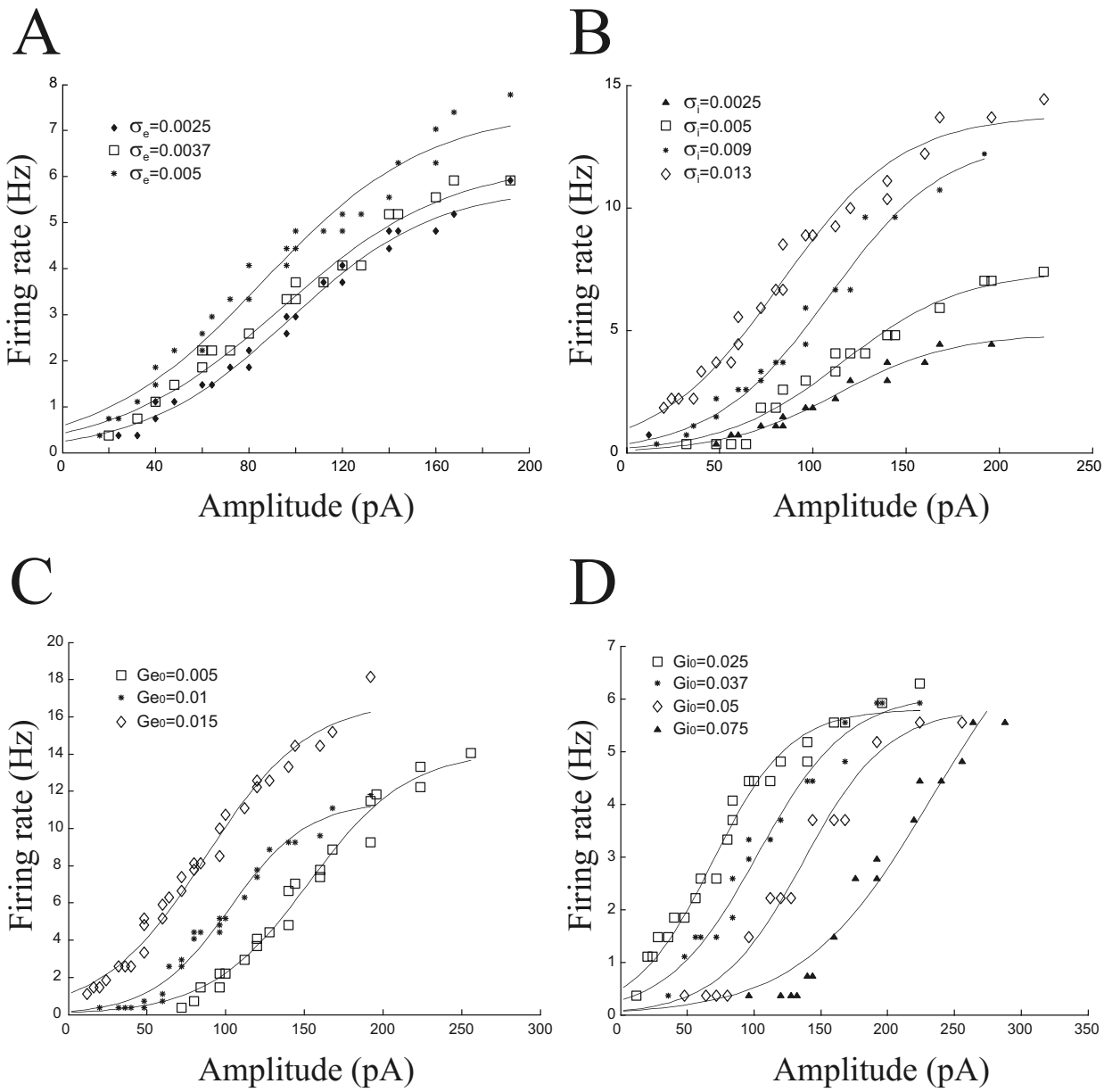

Fig. 9. Influence of the point conductance parameters on the F-I curves of prefrontal cortical cells undergoing simulated synaptic background activity. A: Increases in the S.D. of excitatory inputs slightly increased the slope of the response curves of this cell. B: An increase in the S.D. of inhibitory inputs increased the slope of the response curves (gain of the cell), and increased its maximum firing rate. C: An increase in the mean excitatory inputs shifted the response curves leftward, keeping their slope constant and increasing its maximal value only slightly. D: An increase in the mean inhibitory conductance drive shifted the response curves toward the right, while their slope (gain) and maximal value remain constant. Panels B and C are from the same cell. Panels A and D are from two other cells.

(Destexhe et al., 2001). The cell could detect short increases in the S.D. of the excitatory synaptic drive that mimicked transient increases in the correlation of the inputs, as observed *in vivo* (Azouz and Gray, 1999). The presence of synaptic background activity also allowed the cell to detect transient increases in the S.D. of the excitatory conductances that would otherwise be subthreshold. Using modeling and experimental methods, we determined that the mean inhibitory and excitatory synaptic input levels set the 'working point' of the cell by shifting the F-I curve rightward or leftward respectively. The S.D. of the inhibitory inputs to the cell was the major determinant of its gain.

Recently, Chance et al. (2002) presented experimental and theoretical evidence that synaptic background noise modulates the gain of pyramidal cells of rat somatosensory cortex, consistent with the present study. Both studies used the dynamic clamp technique, but our point-conductance model (see Experimental Procedures) allowed the mean and S.D. of the excitatory and inhibitory synaptic

background activity to be separately manipulated. This allowed the input resistance (set by Gi_0), the subthreshold membrane fluctuation amplitude (set primarily by σ_e), the level of depolarization of the neuron (set by Ge_0) and its gain (set by σ_i) to be independently varied. Consequently, the CV values obtained here were closer to their values measured *in vivo* than those reported in Chance et al. (2002) and the cells were sufficiently adapted that their firing rates rarely exceeded 50 Hz for large current values, as observed in the behaving monkey *in vivo*. The F-I curves of cells in the Chance et al. (2002) study were best fit by a second order polynomial, which inevitably included a 'hard threshold' below which the firing rates are zero. In contrast, in our sample from prefrontal cortex, the cells were best fit by a sigmoid function that had no 'hard' thresholds.

Another difference was that Chance et al. (2002) focused on conditions where the excitatory and inhibitory synaptic conductances were balanced, whereas the present study focused on 'near threshold' conditions where cells have a low spontaneous firing rate, as observed *in vivo*. We showed here that the gain of a cell may be modulated separately by either excitation alone, or inhibition alone. In addition, under these conditions an increase in the S.D. of inhibitory noise resulted primarily in an increase in the gain of the cell (slope of the sigmoid curve at mid-height; Fig. 9A and 9B), whereas Chance et al. (2002) reported that when the excitatory and inhibitory conductances were increased together, there was a decrease in the gain (initial slope of the F-I curve). This decrease was also observed with a simple one-compartmental model that included only I_{Na}, I_{kd} and I_M currents (not shown). The reason for the apparent discrepancy in our conclusions is that large fluctuations of the membrane potential in the hyperpolarizing direction tend to de-inactivate the sodium channels responsible for spike initiation as well as activate hyperpolarization-activated currents such as I_h. This results in a greater sensitivity of the cell (increase in gain) when subsequent excitatory inputs arrive, consistent with earlier studies in which the spike-triggered average shows a hyperpolarization just before a spike (Mainen and Sejnowski, 1995). Large membrane fluctuations (especially those produced by synchronized inhibition) should therefore yield higher sensitivity. This raises the intriguing possibility that noise-induced gain modulation may be different in neurons that have a complex mix of intrinsic conductances that yield low firing rates, such as those in the prefrontal cortex, compared with neurons with high firing rates, as in the somatosensory cortex.

The study of stochastic resonance has established that inputs may be best detected for an optimal amount of somatic current noise (McNamara and Wiesenfeld, 1989; Longtin, 1993; Levin and Miller, 1996; White et al., 1998; Stacey and Durand, 2000). However, cortical neurons *in vivo* are in a 'high conductance' state (Paré et al., 1998; Destexhe and Paré, 1999; Destexhe et al., 2003), and their membrane fluctuations are best described as variability in synaptic conductances rather than variability in somatic currents. Moreover, voltage clamp recordings in the cat visual system *in vivo* showed that the large variations in membrane conductance due to visual inputs was mainly due to a transient ($<$ 50 ms) increase in shunting inhibition (Borg-Graham et al., 1998). Our results show that inhibition was indeed the most effective determinant of membrane input resistance, and that in *in vivo*-like conditions, cells were able to detect transient conductance changes (10–80 ms) of the order of the ones measured *in vivo*.

Recent theoretical work has shown that synaptic background activity enhances the responsiveness of model neurons to inputs that would otherwise stay subthreshold (Hô and Destexhe, 2000). The enhancement by synaptic background noise of the responsiveness of the model cell was robust to changes in the dendritic morphology, distribution of leak currents, the value of axial resistivity, the densities of voltage-dependent current and the spatial distribution of synaptic inputs (Hô and Destexhe, 2000). In this model, the input signal was carried by a set of synapses that were not otherwise active. However, when activated, the correlation of their discharges could be detected in time windows as short as 2 ms (Rudolph and Destexhe, 2001). Consistent with these results, we have shown here that cells placed in *in vivo*-like conditions of synaptic and intrinsic noise are able to detect short signals that would have remained subthreshold without the presence of background synaptic noise (Fig. 7). A higher excitatory synaptic background mean conductance brings the membrane closer to threshold (because the reversal potential for AMPA is at 0 mV) and increases the background firing rate of the cell and its response to a given current pulse (Fig. 9C). Conversely, a higher inhibitory mean conductance pushes the membrane potential away from threshold and reduces the spontaneous firing rate of the cell (Fig. 9D). However, changes in the variances of synaptic background noise do not change the mean conductances or the mean membrane potential, but rather change the fluctuations around the mean (in both directions, for both excitation and inhibition). Therefore, increases in both σ_e and σ_i are capable of inducing depolarizing deviations of the membrane voltage leading to an increase in the probability to cross the spike threshold (Fig. 6).

Pyramidal cells recorded *in vitro* could not detect signals shorter than 10 ms unless they consisted in large variations (more than six-fold) in the S.D. of the background noise. This discrepancy might be due to slow membrane currents, such as h-currents or calcium-dependent potassium currents that were present *in vitro*, but not included in the models. Another difference is in the somatic localization of the point-conductance clamp, whereas synaptic inputs occur on dendrites where they may participate in local interactions with intrinsic conductances. Further work will be needed to evaluate the impact of these different contributions.

Recent experimental work showed that the detection of subthreshold signals could be improved by increasing the background levels of presynaptic firing (Stacey and Durand, 2001). In these slice experiments, synaptic background noise was elicited by extracellular stimulation of the CA3 region of the hippocampus, while an intracellular re-

cording was obtained from a CA1 cell. These results are compatible with ours, even though the levels of synaptic noise were lower than that expected *in vivo*, and even though the input resistance of the CA1 cell during the extracellular stimulation was probably higher than it would have been *in vivo* (Fig. 2). These two shortcomings are inherent to the slice preparation where synaptic inputs are greatly reduced. The method we used here circumvented these shortcomings and allowed the independent control of the excitatory and inhibitory contributions to synaptic inputs.

Correlation of synaptic inputs increases the fluctuations of the membrane potential of the postsynaptic cell. A sustained increase in correlation has predictable consequences on the mean firing rate of the neuron and on its firing variability (Salinas and Sejnowski, 2000; Svirskis and Rinzel, 2000). We showed that responses to sustained increases in their inputs (long current pulses) depended on the variance of the noise while their thresholds for detecting sustained events (′working point') were set by the mean excitatory and inhibitory synaptic drives. The sensitivity (gain) was dynamically set by the S.D. of their inhibitory synaptic inputs. The synaptic background noise coming from the 'context' is therefore a key determinant of the specific signal processing capabilities of the cell. The distinction between the influences of the mean synaptic inputs from the variances of the inputs has important computational consequences for cortical processing, as first explored in Sejnowski (1976, 1981). These results predict that the responsiveness of a given cell may be modulated by the level of synchronization present in its background synaptic inputs. It is in general difficult to modulate *in vivo* the level of background synchrony to a given cell. There is however a useful experimental observation that may be used to test this hypothesis. Under specific kinds of anesthesia, cortical networks spontaneously synchronize at low frequencies (1–2 Hz; Steriade et al., 1993; Contreras and Steriade, 1995; Kisley and Gerstein, 1999). This synchronization occurs with fast onset and smoothly decreases with time in a stereotypical manner and could therefore be used as an *in vivo* assay of background synaptic synchrony. Our results showed that the gain of a cell was positively related (Fig. 9A, B) to the amount of variance (i.e. correlation Fig. 5) in the background synaptic inputs. After each spontaneously discharges, the slope of the input/output curve (gain) would be initially steep (high synchrony) and decrease smoothly. The consequence of this decrease would be that shortly after each spontaneous discharges (small delays) the cells would be very responsive to external stimuli (fast onset, large number of spikes), while later (longer delays, but before a new discharge) the cell's gain would be lower, and the cell would be less responsive (slower onset, smaller number of spikes). These results have indeed been observed *in vivo* in the rat using auditory stimuli that were time locked to these spontaneous discharges (Kisley and Gerstein, 1999).

We limited our study to regularly spiking pyramidal cells. Recent experiments suggest, however, that the detection of synchronous inputs (here simulated by an increase in the S.D. of the synaptic noise) could also be effectively achieved by a network of fast spiking interneurons (Galarreta and Hestrin, 2001). Because interneurons are in general electrotonically more compact, and because their firing rate can potentially be much higher than pyramidal cells, it is likely that their responses to transient or sustained variation in their inputs will be more sensitive to the makeup of the synaptic noise. Interestingly, the electrotonus and firing rates of pyramidal cells can be significantly modulated by substances such as acetylcholine, serotonin, dopamine or norepinephrine that are abundant *in vivo*, but absent in most *in vitro* preparations (Hasselmo, 1995). The exact consequences of various levels of these neurochemical substances is still poorly understood, (see Fellous and Linster, 1998 for a review). It is likely that neuromodulators will change the signal detection abilities of neurons by modulating their gain (Servan-Schreiber et al., 1990) and their sensitivity to transient inputs. Further work is needed to understand how the input/output properties of cells placed in *in vivo* conditions of synaptic inputs are modulated by neuromodulators, and how this gain control compares with the one obtained here by controlling fluctuating synaptic conductances. Our study is also limited by the fact that recordings *in vitro* were performed at the soma. While the OU conductances used here accounted for the passive properties of typical dendritic trees, they did not capture the eventual local dendritic computations that might occur during the course of short or sustained signal transmission (Mel, 1994).

These results show that the makeup of synaptic background noise helps to dynamically determine the input/ouput properties of individual cells. In cortical systems that include feedback projections, this modulation can in principle implement a top-down influence on bottom-up processing. In the visual pathway, for example, this mechanism can be used by 'higher level' processing centers such as the inferotemporal cortex (IT) to modulate the activity of low-level perceptual centers such as V1. An object activating its representation in IT would increase the synchrony of the neural responses of IT neurons. This increase in synchrony would be reflected as an increase in the variance of the background synaptic inputs received by earlier stages of visual processing, through the direct back-projections from IT to V2 or V1. This increase of variance, as we showed, could result in an increase in the gain of these cells, thereby increasing their sensitivity to the stimulus. This mechanism could be used to regulate attention and also enhance signal processing.

Acknowledgements—We thank Darrel Henze and G. Buzsaki (Rutgers University) for their invaluable help with the in vivo experiments. Research was supported by the Howard Hughes Medical Institute, the National Institutes of Health (NIH) and the Centre National pour la Recherche Scientifique (CNRS).

REFERENCES

Azouz R, Gray CM (1999) Cellular mechanisms contributing to response variability of cortical neurons in vivo. J Neurosci 19:2209–2223.

Bair W (1999) Spike timing in the mammalian visual system. Curr Opin Neurobiol 9:447–453.
Barry PH (1994) JPCalc, a software package for calculating liquid junction potential corrections in patch-clamp, intracellular, epithelial and bilayer measurements and for correcting junction potential measurements. J Neurosci Methods 51:107–116.
Barry PH, Lynch JW (1991) Liquid junction potentials and small cell effects in patch-clamp analysis. J Membr Biol 121:101–117.
Bazhenov M, Stopfer M, Rabinovich M, Huerta R, Abarbanel HD, Sejnowski TJ, Laurent G (2001) Model of transient oscillatory synchronization in the locust antennal lobe. Neuron 30:553–567.
Bernander O, Douglas RJ, Martin KA, Koch C (1991) Synaptic background activity influences spatiotemporal integration in single pyramidal cells. Proc Natl Acad Sci USA 88:11569–11573.
Borg-Graham LJ, Monier C, Fregnac Y (1998) Visual input evokes transient and strong shunting inhibition in visual cortical neurons. Nature 393:369–373.
Chance FS, Abbott LF, Reyes AD (2002) Gain modulation from background synaptic input. Neuron 35:773–782.
Contreras D, Steriade M (1995) Cellular basis of EEG slow rhythms: a study of dynamic corticothalamic relationships. J Neurosci 15:604–622.
Contreras D, Timofeev I, Steriade M (1996) Mechanisms of long-lasting hyperpolarizations underlying slow sleep oscillations in cat corticothalamic networks. J Physiol 494:251–264.
deCharms RC, Zador A (2000) Neural representation and the cortical code. Annu Rev Neurosci 23:613–647.
DeFelipe J, Fariñas I (1992) The pyramidal neuron of the cerebral cortex: morphological and chemical characteristics of the synaptic inputs. Prog Neurobiol 39:563–607.
Destexhe A, Mainen ZF, Sejnowski TJ (1994) Synthesis of models for excitable membranes, synaptic transmission and neuromodulation using a common kinetic formalism. J Comput Neurosci 1:195–230.
Destexhe A, Paré D (1999) Impact of network activity on the integrative properties of neocortical pyramidal neurons in vivo. J Neurophysiol 81:1531–1547.
Destexhe A, Rudolph M, Fellous JM, Sejnowski TJ (2001) Fluctuating synaptic conductances recreate in vivo-like activity in neocortical neurons. Neuroscience 107:13–24.
Destexhe, A, Rudolph, M, Pare, D (2003) The high-conductance state of neocortical neurons in vivo. Nat Rev Neurosci 4:739–751.
Fabre-Thorpe M, Delorme A, Marlot C, Thorpe S (2001) A limit to the speed of processing in ultra-rapid visual categorization of novel natural scenes. J Cogn Neurosci 13:171–180.
Fellous JM, Houweling AR, Modi RH, Rao RP, Tiesinga PH, Sejnowski TJ (2001) Frequency dependence of spike timing reliability in cortical pyramidal cells and interneurons. J Neurophysiol 85:1782–1787.
Fellous J-M, Linster C (1998) Computational models of neuromodulation. Neural computation 10:771–805.
Fries P, Reynolds JH, Rorie AE, Desimone R (2001) Modulation of oscillatory neuronal synchronization by selective visual attention. Science 291:1560–1563.
Galarreta M, Hestrin S (2001) Spike transmission and synchrony detection in networks of GABAergic interneurons. Science 292:2295–2299.
Gawne TJ, Richmond BJ (1993) How independent are the messages carried by adjacent inferior temporal cortical neurons? J Neurosci 13:2758–2771.
Gillespie DT (1996) The mathematics of Brownian motion and Johnson noise. Am J Physics 64:225–240.
Hasselmo ME (1995) Neuromodulation and cortical function: modeling the physiological basis of behavior. Behav Brain Res 67:1–27.
Henze DA, Borhegyi Z, Csicsvari J, Mamiya A, Harris KD, Buzsaki G (2000) Intracellular features predicted by extracellular recordings in the hippocampus in vivo. J Neurophysiol 84:390–400.
Hines ML, Carnevale NT (1997) The NEURON simulation environment. Neural Comput 9:1179–1209.
Hô N, Destexhe A (2000) Synaptic background activity enhances the responsiveness of neocortical pyramidal neurons. J Neurophysiol 84:1488–1496.
Holt GR, Softky WR, Koch C, Douglas RJ (1996) Comparison of discharge variability in vitro and in vivo in cat visual cortex neurons. J Neurophysiol 75:1806–1814.
Hughes SW, Cope DW, Crunelli V (1998) Dynamic clamp study of Ih modulation of burst firing and delta oscillations in thalamocortical neurons in vitro. Neuroscience 87:541–550.
Huguenard JR, Hamill OP, Prince DA (1988) Developmental changes in Na^+ conductances in rat neocortical neurons: appearance of a slowly inactivating component. J Neurophysiol 59:778–795.
Jaeger D, Bower JM (1999) Synaptic control of spiking in cerebellar Purkinje cells: dynamic current clamp based on model conductances. J Neurosci 19:6090–6101.
Keysers C, Xiao DK, Foldiak P, Perrett DI (2001) The speed of sight. J Cogn Neurosci 13:90–101.
Kisley MA, Gerstein GL (1999) Trial-to-trial variability and state-dependent modulation of auditory-evoked responses in cortex. J Neurosci 19:10451–10460.
Larkman AU (1991) Dendritic morphology of pyramidal neurones of the visual cortex of the rat: III. Spine distributions. J Comp Neurol 306:332–343.
Levin JE, Miller JP (1996) Broadband neural encoding in the cricket cercal sensory system enhanced by stochastic resonance. Nature 380:165–168.
Lewis BL, O'Donnell P (2000) Ventral tegmental area afferents to the prefrontal cortex maintain membrane potential 'up' states in pyramidal neurons via D(1) dopamine receptors. Cereb Cortex 10:1168–1175.
Longtin A (1993) Stochastic resonance in neuron models. J Stat Physics 70:309–327.
Lytton WW (1996) Optimizing synaptic conductance calculation for network simulations. Neural Comput 8:501–509.
Mainen ZF, Sejnowski TJ (1995) Reliability of spike timing in neocortical neurons. Science 268:1503–1506.
McAllister AK, Stevens CF (2000) Nonsaturation of AMPA and NMDA receptors at hippocampal synapses. Proc Natl Acad Sci USA 97:6173–6178.
McNamara B, Wiesenfeld K (1989) Theory of stochastic resonance. Phys Rev A 39:4854–4869.
Mel BW (1994) Information processing in dendritic trees. Neural Comput 6:1031–1085.
Neher E (1995) Voltage offsets in Patch-clamp experiments. In: Single-channel recording (Sakmann B, Neher E, eds), pp 147–153. New York: Plenum Press.
Nelder JA, Mead R (1965) A simplex method for function minimization. Comput J 7:308–313.
Paré D, Shink E, Gaudreau H, Destexhe A, Lang EJ (1998) Impact of spontaneous synaptic activity on the resting properties of cat neocortical pyramidal neurons in vivo. J Neurophysiol 79:1450–1460.
Reinagel P, Reid RC (2002) Precise firing events are conserved across neurons. J Neurosci 22:6837–6841.
Rudolph M, Destexhe A (2001) Correlation detection and resonance in neural systems with distributed noise sources. Phys Rev Lett 86:3662–3665.
Salinas E, Sejnowski TJ (2000) Impact of correlated synaptic input on output firing rate and variability in simple neuronal models. J Neurosci 20:6193–6209.
Salinas E, Sejnowski TJ (2001) Correlated neuronal activity and the flow of neural information. Nat Rev Neurosci 2:539–550.
Sejnowski TJ (1976) On the stochastic dynamics of neuronal interaction. Biol Cybern 22:203–211.
Sejnowski TJ (1981) Skeleton filters in the brain; parallel models of associative memory. Hillsdale, New Jersey: Lawrence Erlbaum Associates.
Servan-Schreiber D, Printz H, Cohen JD (1990) A network model of

catecholamine effects: gain, signal-to-noise ratio, and behavior. Science 249:892–895.
Shadlen MN, Newsome WT (1994) Noise, neural codes and cortical organization. Curr Opin Neurobiol 4:569–579.
Shadlen MN, Newsome WT (1998) The variable discharge of cortical neurons: implications for connectivity, computation, and information coding. J Neurosci 18:3870–3896.
Sharp AA, O'Neil MB, Abbott LF, Marder E (1993) Dynamic clamp: computer-generated conductances in real neurons. J Neurophysiol 69:992–995.
Softky WR, Koch C (1993) The highly irregular firing of cortical cells is inconsistent with temporal integration of random EPSPs. J Neurosci 13:334–350.
Stacey WC, Durand DM (2000) Stochastic resonance improves signal detection in hippocampal CA1 neurons. J Neurophysiol 83:1394–1402.
Stacey WC, Durand DM (2001) Synaptic noise improves detection of subthreshold signals in hippocampal CA1 neurons. J Neurophysiol 86:1104–1112.
Steinmetz PN, Roy A, Fitzgerald PJ, Hsiao SS, Johnson KO, Niebur E (2000) Attention modulates synchronized neuronal firing in primate somatosensory cortex. Nature 404:187–190.
Steriade M, Nunez A, Amzica F (1993) A novel slow ($<$1 Hz) oscillation of neocortical neurons in vivo: depolarizing and hyperpolarizing components. J Neurosci 13:3252–3265.
Svirskis G, Rinzel J (2000) Influence of temporal correlation of synaptic input on the rate and variability of firing in neurons. Biophys J 79:629–637.
Tiesinga PH, Jose JV, Sejnowski TJ (2000) Comparison of current-driven and conductance-driven neocortical model neurons with Hodgkin-Huxley voltage-gated channels. Phys Rev E Stat Phys Plasmas Fluids Relat Interdiscip Topics 62:8413–8419.
Traub RD, Miles R (1991) Neuronal networks of the hippocampus. Cambridge, UK: Cambridge University Press.
Troyer TW, Miller KD (1997) Physiological gain leads to high ISI variability in a simple model of a cortical regular spiking cell. Neural Comput 9:971–983.
Uhlenbeck GE, Ornstein LS (1930) On the theory of Brownian motion. Phys Rev 36:823–841.
Watt AJ, van Rossum MC, MacLeod KM, Nelson SB, Turrigiano GG (2000) Activity coregulates quantal AMPA and NMDA currents at neocortical synapses. Neuron 26:659–670.
White EL (1989) Cortical circuits. Boston: Birkhauser.
White JA, Klink R, Alonso A, Kay AR (1998) Noise from voltage-gated ion channels may influence neuronal dynamics in the entorhinal cortex. J Neurophysiol 80:262–269.
Zador A (1998) Impact of synaptic unreliability on the information transmitted by spiking neurons. J Neurophysiol 79:1219–1229.
Zador A (1999) Thalamocortical synapses: sparse but stentorian. Neuron 23:198–200.

(Accepted 21 August 2003)